Article

Cell Reports

DEAD-Box Helicase 18 Counteracts PRC2 to Safeguard Ribosomal DNA in Pluripotency Regulation

Graphical Abstract

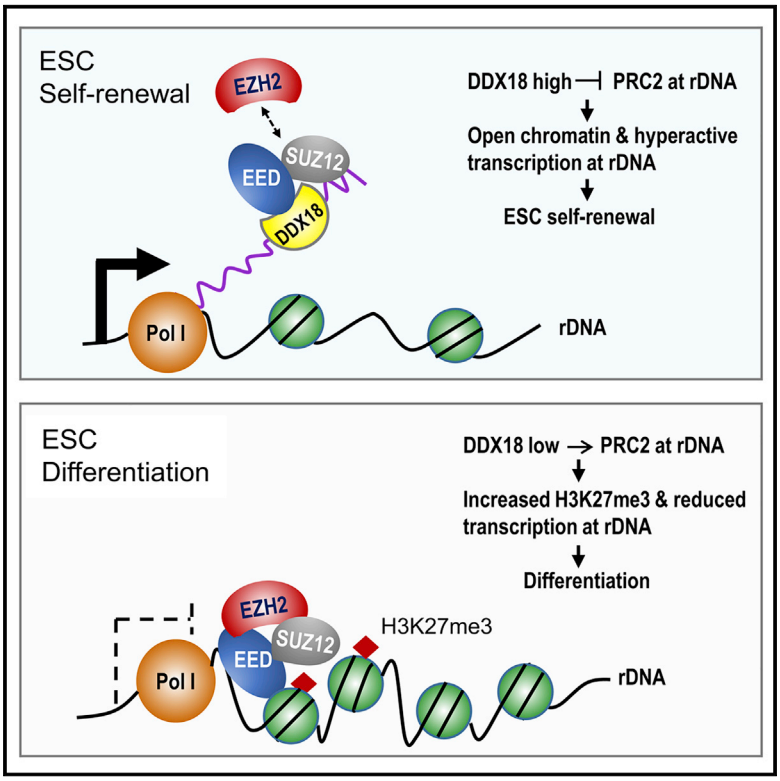

Highlights

- DDX18 is essential for ESC self-renewal and embryonic development
- DDX18 directly binds PRC2 and modulates PRC2 complex formation
- DDX18 prevents PRC2 from accessing rDNA in the nucleolus
- DDX18 promotes open chromatin and hyperactive transcription at rDNA

Authors

Hui Zhang, Zhongyang Wu, J. Yuyang Lu, ..., Wei Xie, Jianlong Wang, Xiaohua Shen

Correspondence

biozhanghui@aliyun.com (H.Z.), xshen@tsinghua.edu.cn (X.S.)

In Brief

Zhang et al. report an interplay between the DEAD-box helicase DDX18 and the polycomb repressive complex 2 (PRC2) in governing the hyperactive state of ribosomal DNA in pluripotency regulation. DDX18 counteracts PRC2 complex formation and prevents PRC2 binding and aberrant histone methylation at rDNA loci.

Zhang et al., 2020, Cell Reports *30*, 81–97
January 7, 2020
https://doi.org/10.1016/j.celrep.2019.12.021

CellPress

Cell Reports
Article

DEAD-Box Helicase 18 Counteracts PRC2 to Safeguard Ribosomal DNA in Pluripotency Regulation

Hui Zhang,[1,3,*] Zhongyang Wu,[1,3] J. Yuyang Lu,[1,3] Bo Huang,[1] Hongwei Zhou,[2,4] Wei Xie,[1] Jianlong Wang,[2,4] and Xiaohua Shen[1,5,*]

[1]Tsinghua Center for Life Sciences, Department of Basic Medical Sciences in School of Medicine, and School of Life Sciences, Tsinghua University, Beijing 100084, China
[2]The Black Family Stem Cell Institute and Department of Cell, Developmental, and Regenerative Biology, Icahn School of Medicine at Mount Sinai, New York, NY, USA
[3]These authors contributed equally
[4]Present address: Department of Medicine, Columbia Center for Human Development, Columbia University Irving Medical Center, New York, NY 10032, USA
[5]Lead Contact
*Correspondence: biozhanghui@aliyun.com (H.Z.), xshen@tsinghua.edu.cn (X.S.)
https://doi.org/10.1016/j.celrep.2019.12.021

SUMMARY

Embryonic stem cells (ESCs) exhibit high levels of ribosomal RNA (rRNA) transcription and ribosome biogenesis. Here, we reveal an unexpected role for an essential DEAD-box helicase, DDX18, in antagonizing the polycomb repressive complex 2 (PRC2) to prevent deposition of the repressive H3K27me3 mark onto rDNA in pluripotent cells. DDX18 binds and sequesters PRC2 in the outer layer of the nucleolus and counteracts PRC2 complex formation *in vivo* and *in vitro*. *DDX18* knockdown leads to increased occupancy of PRC2 and H3K27me3 at rDNA loci, accompanied by drastically decreased rRNA transcription and reduced ribosomal protein expression and translation. Auxin-induced rapid degradation of DDX18 enhances PRC2 binding at rDNA. The inhibition of PRC2 partially rescues the effects of *DDX18* depletion on rRNA transcription and ESC self-renewal. These results demonstrate a critical role for DDX18 in safeguarding the chromatin and transcriptional integrity of rDNA by counteracting the epigenetic silencing machinery to promote pluripotency.

INTRODUCTION

Embryonic stem cells (ESCs), derived from the inner cell mass (ICM) of pre-implantation blastocysts, are rapidly proliferating pluripotent cells that are characterized by their remarkable ability to self-renew and differentiate into all somatic cells in *in vitro* culture. Compared to differentiated cells, ESCs feature a globally permissive chromatin structure and an enormously large nucleolus and exhibit hyperactive transcription and high levels of ribosome biogenesis (Gaspar-Maia et al., 2011; Niwa, 2007; Percharde et al., 2017). Recently, emerging lines of evidence have linked ribosomal RNA (rRNA) transcription to ESC self-renewal and early mammalian development. For example, HIRA/H3.3-dependent rRNA transcription is required for zygotic development past the first cleavage (Lin et al., 2014). LINE1 retrotransposons promote rRNA synthesis and play essential roles in ESCs and pre-implantation embryos (Percharde et al., 2018). In ESCs, high levels of rRNA transcription, ribosome biogenesis, and protein translation support the accelerated proliferation required for ESC self-renewal (Corsini et al., 2018; Percharde et al., 2017; You et al., 2015). Accordingly, repression of rDNA transcription and perinucleolar heterochromatin formation are critical for exit from pluripotency and appropriate differentiation (Savić et al., 2014). However, the requirement for the regulation of rRNA transcription and ribosome biogenesis, once regarded as housekeeping processes, has yet to be explored in ESCs.

The nucleolus is best known as the site of rRNA transcription and ribosome biogenesis, in which >200 proteins coordinate to synthesize and process rRNAs, and then assemble those rRNAs with the ribosomal proteins. The nucleolus comprises three principal functional components known as the fibrillar center (FC, innermost), the dense fibrillar component (DFC, intermediate), and the granular compartment (GC, outermost), in which transcription of the rDNA, rRNA processing, and ribosome assembly occur, respectively (Cisterna and Biggiogera, 2010). Human and mouse genomes comprise 200–300 copies of ribosomal DNA (rDNA) genes that are clustered in tandem repeats on the short arms of up to 6 acrocentric chromosomes (McStay, 2016). The rDNA genes are transcribed by RNA polymerase I (Pol I) to generate an ~13-kb (45S/47S) precursor rRNA (pre-rRNA), which is modified and cleaved to produce 28S, 18S, and 5.8S rRNAs (Boisvert et al., 2007; McStay, 2016). The epigenetic state of rDNA is correlated with its transcription activity (Grummt and Längst, 2013). Euchromatic histone marks are associated with actively transcribed rDNA genes, whereas heterochromatin marks, such as trimethylation on histone H3 at lysine 27 (H3K27me3) and H3K9 dimethylation (H3K9me2), are found in silenced rDNA loci (Cong et al., 2012). Dynamic repression of rRNA transcription through the formation of heterochromatin at the rDNA loci has been reported in response to energy deprivation (Grummt and Längst, 2013; Murayama et al., 2008; Zhou et al., 2009). However, the mechanisms that safeguard the rDNA loci from epigenetic silencing in undifferentiated ESCs remain less well understood.

DEAD-box RNA helicase family proteins are abundantly present in all eukaryotic cells and are involved in many steps of RNA

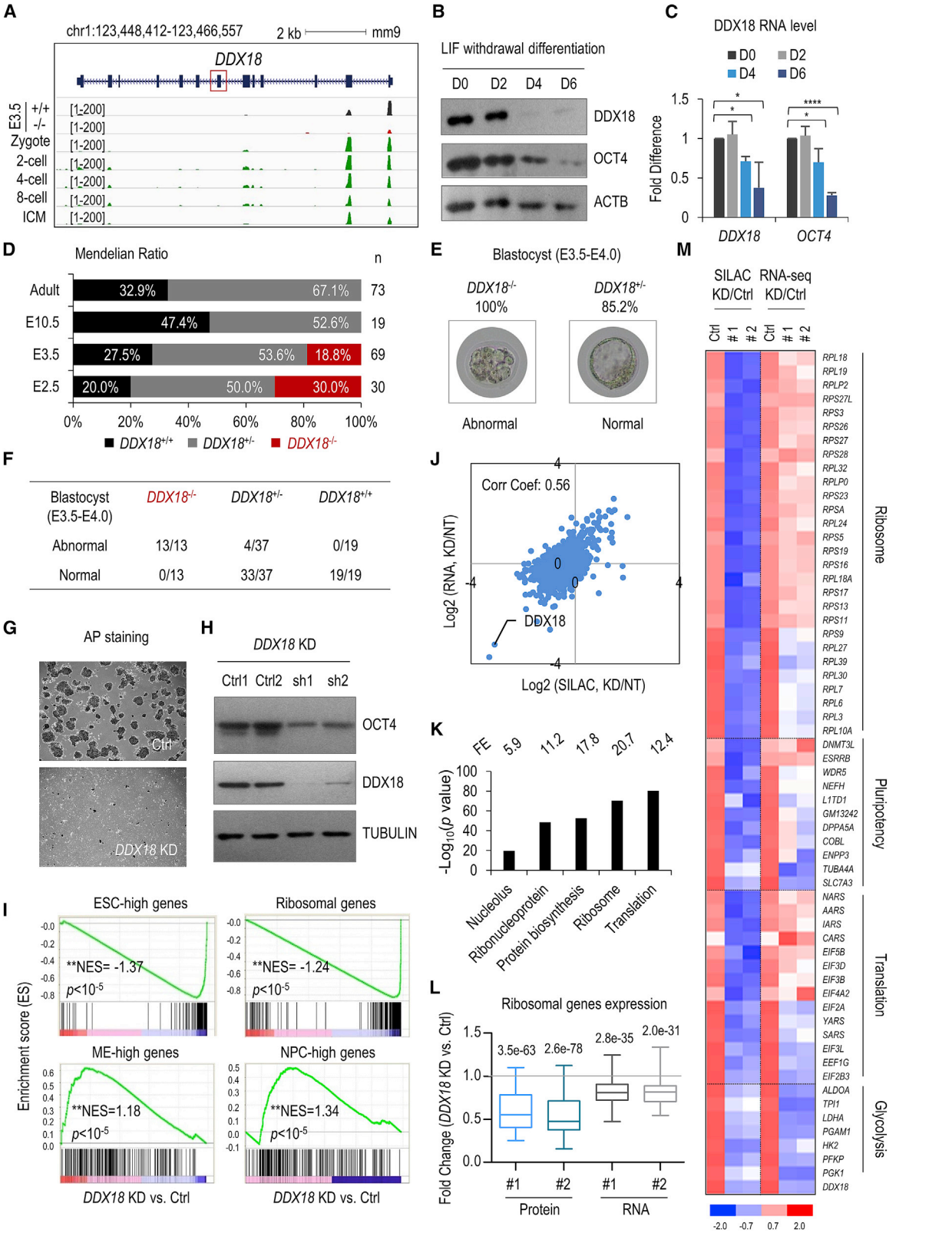

(legend on next page)

metabolism, from RNA transcription to degradation (Jankowsky, 2011; Linder and Jankowsky, 2011). DEAD-box RNA helicase 18 (DDX18) is a highly conserved protein, whose ortholog in yeast, HAS1, is essential for ribosome biogenesis by regulating maturation and processing steps for the assembly of 40S and 60S ribosomal subunits (Dembowski et al., 2013; Emery et al., 2004; Woolford and Baserga, 2013). DDX18 has been reported to be essential for cell-cycle progression in primitive hematopoiesis in zebrafish, and *DDX18* gene mutations have been found in humans with hematologic malignancies (Payne et al., 2011). A previous RNA interference (RNAi) screen in ESCs revealed that knockdown of DDX18 impaired ESC viability (Fazzio et al., 2008). However, the function and mechanism of action of mammalian DDX18 beyond its presumed role in ribosomal assembly remain unclear. The polycomb repressive complex 2 (PRC2), which catalyzes methylations on H3K27, is highly expressed in ESCs and has been linked to the execution of ESC pluripotency (Shen et al., 2008, 2009). Here, we reveal an unforeseen role of DDX18 in the regulation of ESC pluripotency by antagonizing PRC2 activity to safeguard the chromatin integrity of actively transcribed rDNA loci, thereby promoting the hyperactive rRNA transcription and ribosome biogenesis that are required for ESC self-renewal.

RESULTS

Knockout of *DDX18* Leads to Pre-implantation Arrest and Embryonic Lethality

The level of DDX18 expression appears to be tightly regulated during development, with the highest expression in pre-implantation embryos from the zygote to the ICM of blastocyst and the lowest in somatic tissues (Figures 1A and S1A). DDX18 is also abundantly expressed in ESCs, and shows decreased expression at both the RNA and protein levels during ESC differentiation, although more dramatic reduction occurs at the protein level (Figures 1B, 1C, and S1B). The high level of DDX18 expression in embryonic cells prompted us to explore its physiological importance in pluripotency regulation.

We knocked out *DDX18* in mouse by deleting exon 7, which resulted in a frameshift and loss-of-function mutation (Figures S1C–S1G). $DDX18^{+/-}$ heterozygous mice are viable with no apparent phenotypic abnormalities. However, heterozygote intercrosses failed to produce viable homozygous $DDX18^{-/-}$ newborn offspring (Figures 1D, S1F, and S1G). Further analysis showed that $DDX18^{-/-}$ embryos were detected at embryonic day (E) 3.5 with a frequency of 18.8%, but no viable $DDX18^{-/-}$ embryos were found at E10.5 (Figure 1D). At E3.5–E4.0, $DDX18^{-/-}$ embryos were apparently arrested at the morula stage and failed to form distinct blastocoels, whereas their wild-type (WT) or heterozygote littermates developed into blastocysts (Figures 1E, 1F, S1H, and S1I). This indicates peri-implantation arrest and lethality.

To characterize the molecular defects caused by the loss of *DDX18*, we performed an RNA sequencing (RNA-seq) analysis of embryos at E3.5. Compared to WT littermates, $DDX18^{-/-}$ embryos exhibit profound transcriptomic changes of 1,171 genes (fragments per kilobase million [FPKM] >1, absolute fold change >1.5, $p < 0.05$), with 952 downregulated and 219 upregulated (Figure S2A; Table S1). Heatmap and gene set enrichment analysis (GSEA) showed significant downregulation of a set of genes that is highly expressed in ESCs (referred to as ESC-high genes) (Shen et al., 2008, 2009), including *NANOG*, *SALL4*, *ZFP42*, *TET1*, and *TET2* (Figures S2B and S2C). In addition to this decrease in pluripotency transcripts, $DDX18^{-/-}$ embryos exhibited the altered expression of genes involved in embryo development, cell cycle, and ribosome functions (Figure S2B). These results indicated an essential requirement for DDX18 in the acquisition of pluripotency in early development.

Depletion of *DDX18* Impairs the Self-Renewal and Expression of Ribosomal and Pluripotency Genes in ESCs

To study the role of DDX18 in maintaining pluripotency, we successfully knocked down *DDX18* by two small hairpin RNAs (shRNAs) in ESCs (Figure S2D). The depletion of *DDX18* reduced the protein levels of OCT4 and SOX2 and dramatically impaired ESC proliferation as detected by alkaline phosphatase (AP) staining (Figures 1G, 1H, and S2D). RNA-seq profiling revealed profound expression changes of 2,047 genes (FPKM >1, fold change >2 or <−1.5, $p < 0.05$) upon knockdown of *DDX18* (Table S1). The downregulated genes (1,001) are significantly enriched

Figure 1. DDX18 Is Essential for Establishing Pluripotency during Embryogenesis and for Pluripotency Maintenance in ESCs

(A) Genome browser view of the *DDX18* locus. Deep sequencing tracks are displayed below to show the levels of *DDX18* mRNA in wild-type (WT, +/+) and homozygous *DDX18* knockout (KO, −/−) embryos (E3.5). Expression of *DDX18* in zygotes, 2-cell, 4-cell, and 8-cell stage embryos and ICM are also shown (Wu et al., 2016). The red box marks the deleted exon 7 of DDX18 in $DDX18^{-/-}$ mice.

(B and C) DDX18 protein and RNA levels are reduced during ESC differentiation induced by leukemia inhibitory factor (LIF) withdrawal for the indicated time periods (0, 2, 4, and 6 days), as detected by western blot (B) and qRT-PCR (C). Data are presented as means ± SDs of 3 independent biological replicates. $^{*}p < 0.05$, $^{****}p < 0.00001$.

(D) Survival analysis of $DDX18^{+/-}$ heterozygous mouse intercrosses at 4 developmental stages (E2.5, E3.5, E10.5, and adult).

(E and F) Summary of morphological observations (E) and statistical analyses (F) of blastocysts (E3.5–E4.0) isolated from $DDX18^{+/-}$ intercrosses.

(G and H) *DDX18* depletion affects ESC self-renewal. Alkaline phosphatase (AP) staining shows that *DDX18* depletion affects ESC self-renewal (G). DDX18 and OCT4 protein levels after 60 h of *DDX18* knockdown (KD) are downregulated, as detected by western blot (H).

(I) *DDX18* depletion impairs ESC pluripotency and expression of genes encoding ribosomal proteins. Gene set enrichment analysis (GSEA) of RNA-seq data with normalized enrichment score (NES) and the nominal p value are shown. ME, mesendoderm; NPCs, neural progenitor cells.

(J) Correlation plot ($p = 8.19 \times 10^{-134}$) comparing mRNA and protein expression changes following *DDX18* KD.

(K) Ribosomal and translational proteins are enriched in the proteins that are downregulated by *DDX18* depletion. Gene Ontology (GO) analysis of genes whose protein products are downregulated in *DDX18*-depleted ESCs. Selected GO terms (fold enrichment [FE] > 5, $p < 1 \times 10^{-15}$) are shown.

(L) Ribosome-associated genes are downregulated at both the RNA and protein levels.

(M) Heatmap of expression changes of proteins and mRNAs following *DDX18* depletion. Representative genes associated with ribosome, pluripotency, translation, and glycolysis functions are shown.

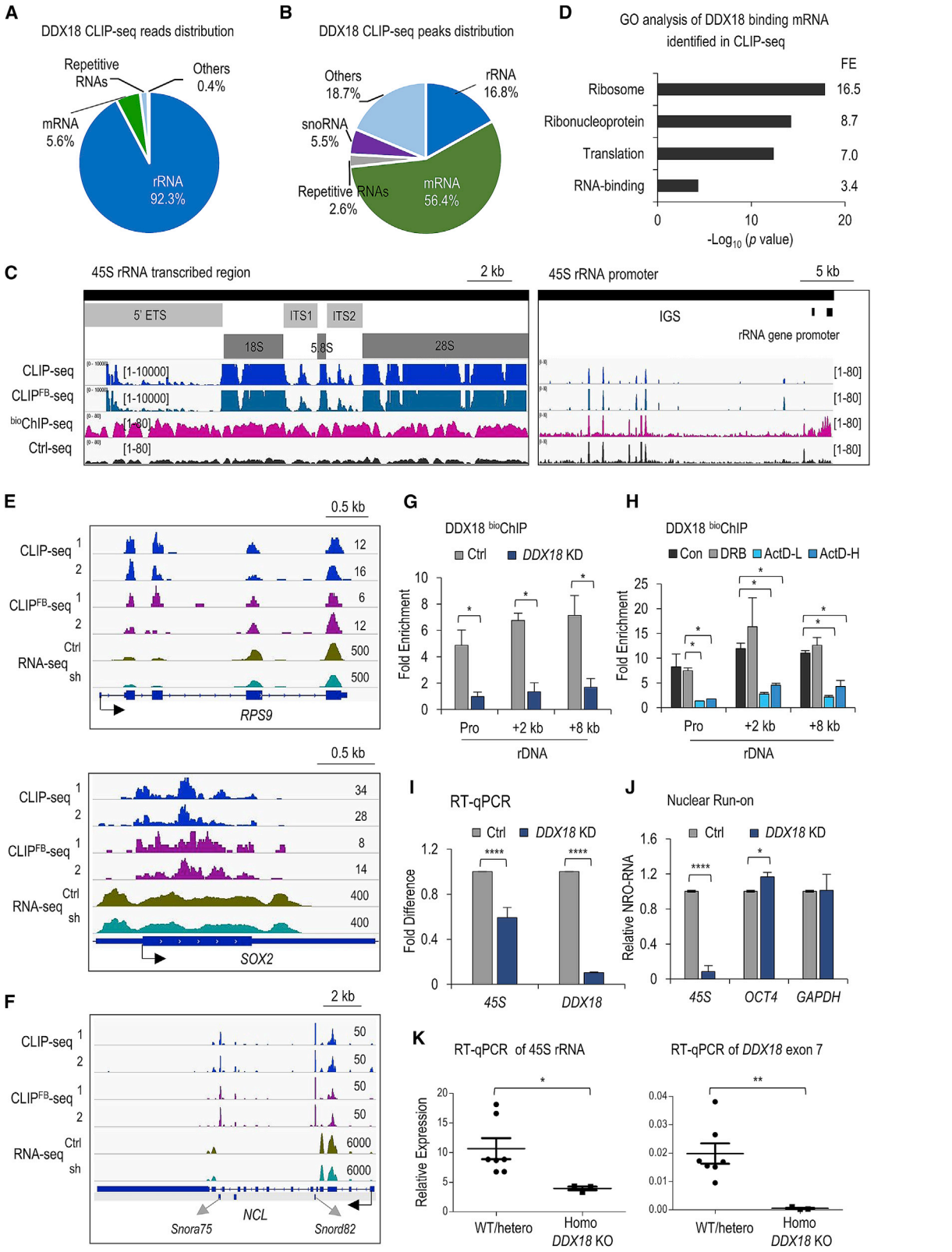

(legend on next page)

in functions related to the ESC-specific expression program, ribosomes, and translation (Figures 1I and S2E). By contrast, the upregulated genes (1,046) are mainly associated with p53 signaling and developmental processes (Figure S2E); they include genes highly expressed in mesendoderm (ME) and neural progenitor cell (NPC) lineages (Figure 1I). This indicates precocious differentiation and impaired self-renewal in ESCs depleted of *DDX18*.

The observation of decreased transcript levels of genes associated with ribosomes led us to examine the effect of *DDX18* depletion on protein synthesis. To measure nascent protein synthesis, we treated ESCs with *O*-propargyl-puromycin (OP-puro), which can be incorporated into newly translated proteins (Bi et al., 2019). OP-puro labeling of ESCs indicated a globally reduced translation rate upon DDX18 knockdown (Figure S2F). To identify proteins with altered abundance, we performed stable isotope labeling using amino acids in cell culture (SILAC) followed by mass spectrometry (MS) sequencing (Figure S2G). The level of DDX18 protein was decreased ~8-fold in *DDX18*-knockdown ESCs, validating the effectiveness of DDX18 depletion and SILAC labeling (Figure 1J). Overall, we detected consistent expression changes at the RNA and protein levels with a correlation coefficient of 0.56 between SILAC and RNA-seq analyses (Figure 1J; Table S2).

Of the 2,337 proteins detected by SILAC, ~423 proteins that overlapped in 2 independent replicates were downregulated >1.5-fold, whereas only 25 proteins were upregulated (Figure S2H; Table S2). This demonstrates a role for DDX18 in promoting global protein synthesis. Congruently, these downregulated proteins are highly enriched in functions related to ribosomes, translation, and the nucleolus (Figure 1K). Global downregulation of ribosome-associated genes was observed at both the RNA and protein levels (Figures 1I and 1L). Notably, for some ribosomal components (e.g., RPL18, RPS5) and pluripotency regulators (e.g., OCT4, SOX2, DPPA5A, ESRRB), the degree of downregulation was more dramatic at the protein level than at the RNA level (Figures 1H, 1M, S2D, and S2H). Thus, transcriptomic and proteomic analyses revealed a critical role for DDX18 in pluripotency maintenance by promoting expression programs involved in pluripotency regulation, ribosome biogenesis, and translation at the levels of transcription and/or translation.

DDX18 Binds Nascent rRNAs and Promotes rDNA Transcription

To explore the mechanisms underlying DDX18-mediated pluripotency regulation, we first sought to define the RNA targets of DDX18 in ESCs. Using an ESC line that stably expresses ectopic DDX18 with amino-terminal FLAG and biotin tags (referred to as DDX18^{FB}) (Figure S3A), we performed FLAG antibody-mediated CLIP-seq (crosslinking and immunoprecipitation followed by sequencing), and FLAG- and biotin-mediated tandem affinity purification followed by CLIP-seq (CLIP^{FB}-seq) (Bi et al., 2019; Liu et al., 2019). These two independent approaches yielded similar results (Figures 2A, 2B, and S3B–S3D; Table S3).

More than 90% of reads (or >16% of peaks) in DDX18 CLIP-seq and CLIP^{FB}-seq mapped to *45S* rRNA (Figures 2A, 2B, S3B, and S3C). While the highest CLIP and CLIP^{FB} signals reside in the gene body of *18S*, *5.8S*, and *28S* transcripts, DDX18 also binds strongly to the 5′ external transcribed spacer (5′ ETS) and internal transcribed spacer (ITS) regions of nascent rRNA (Figures 2C and S3E). Approximately 6%–7% of the CLIP and CLIP^{FB} reads (47%–56% of the peaks) mapped to >177 mRNA transcripts (Figures 2A, 2B, and S3B–S3D), including those encoding the pluripotency regulators OCT4 and SOX2, ribosomal proteins such as RPS5 and RPS9, and the translation regulators EEF1A1 and EEF2 (Figures 2D, 2E, and S3F). In addition, 6%–8% of CLIP and CLIP^{FB} peaks mapped to >46 small nucleolar RNAs (snoRNAs) (Figures 2B, 2F, S3C, S3D, and S3G), which make up approximately one-third of the total of 150 snoRNAs annotated in the mouse (Lestrade and Weber, 2006). These results suggest that DDX18 may be involved in multiple steps of rRNA synthesis, processing, and assembly through its direct associations with its target transcripts.

To test whether DDX18 resides in the proximity of rDNA chromatin, we performed biotin-mediated chromatin immunoprecipitation of DDX18^{FB} followed by quantitative PCR (qPCR) or sequencing (^{bio}ChIP-qPCR or ^{bio}ChIP-seq). Enriched DDX18

Figure 2. DDX18 Binds Nascent rRNAs and Promotes rRNA Transcription

(A and B) Distribution of DDX18-CLIP-seq reads (A) and peaks (B).

(C) A genome browser view of the rDNA locus shows that DDX18 binds to pre-rRNA and rDNA. The rRNA gene promoter; intergenic spacer (IGS); pre-rRNA (*45S*) containing an external transcribed spacer (5′ ETS); two internal transcribed spacers (ITS1 and ITS2); and the *28S*, *5.8S*, and *18S* are labeled. Deep-sequencing tracks from DDX18-CLIP-seq, CLIP^{FB}-seq, and ChIP-seq are shown.

(D) GO analysis of DDX18-associated mRNAs identified by CLIP-seq. Selected GO terms (FE > 3, $p < 1 \times 10^{-4}$) are shown.

(E and F) Gene browser snapshots of representative mRNAs (E) and snoRNAs (F). Deep-sequencing tracks from CLIP-seq, CLIP^{FB}-seq, and RNA-seq are displayed.

(G) DDX18 enrichment at rDNA loci. ^{bio}ChIP-qPCR shows DDX18 enrichment at the rDNA promoter (Pro) and gene body (+2 kb, +8 kb) regions with or without *DDX18* KD.

(H) DDX18 enrichment at rDNA loci is dependent on Pol I transcription. ^{bio}ChIP-qPCR shows DDX18 occupancy at the rDNA loci with or without treatment of the Pol I inhibitor (ActD-L, 50 ng/mL, 2 h; ActD-H, 1 μg/mL, 2 h) or the Pol II inhibitor (DRB, 25 μM, 2 h) (n = 2).

(G and H) Fold enrichment of DDX18 at rDNA regions is normalized to the *GAPDH* (G) or *ACTB* (H) promoters, as determined by ^{bio}ChIP-qPCR.

(I) Abundance of steady-state pre-rRNA (*45S*) decreases with *DDX18* depletion. *45S* was detected by RT-qPCR and is normalized to *ACTB*.

(J) Transcription of nascent rRNA (pre-rRNA) is dramatically downregulated upon *DDX18* KD. *45S* transcription was detected using nuclear run-on (NRO) assays followed by RT-qPCR normalized to *ACTB* pre-mRNA.

(K) Pre-rRNA is reduced in E3.5 *DDX18*$^{-/-}$ embryos. RT-qPCR was performed to detect *45S* and *DDX18* exon 7 in E3.5 WT, heterozygous, or homozygous *DDX18* KO mouse embryos.

Unless otherwise indicated, data are presented as means ± SDs of at least 3 independent biological replicates. *p < 0.05, **p < 0.001, ****p < 0.00001 compared to the control.

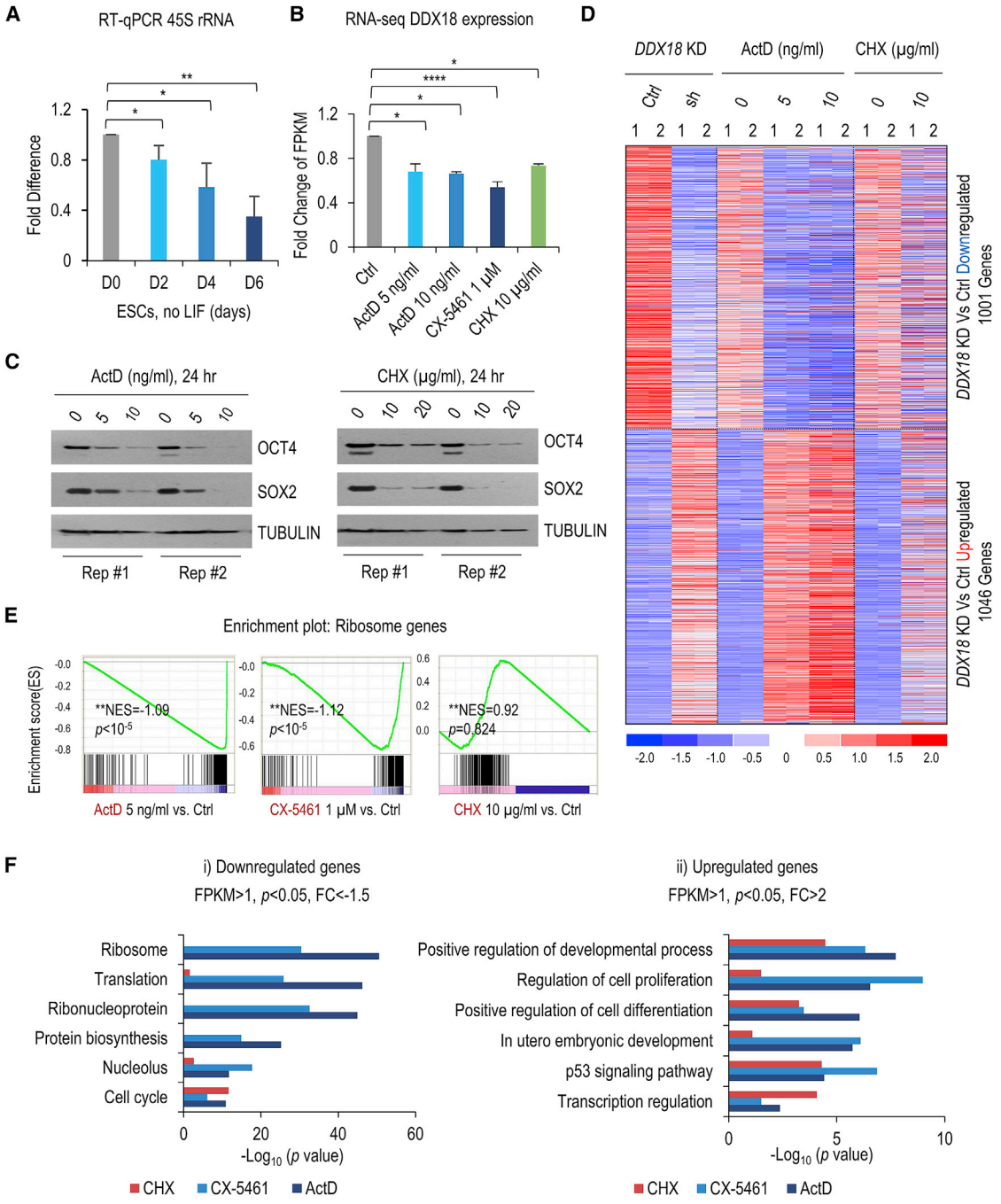

Figure 3. *DDX18* Depletion Mimics Inhibitors of rRNA Transcription by Inhibiting ESC Pluripotency and the Expression of Genes Encoding Ribosome Proteins

(A) The synthesis of rRNA is downregulated during ESC differentiation.

(B) *DDX18* expression is decreased after rRNA transcription inhibition and translation inhibition. *DDX18* expression levels were evaluated by RNA-seq analysis in ActD-, CX-5461-, and CHX-treated ESCs. Data are presented as means ± SDs of at least 2 independent biological replicates. *p < 0.05, **p < 0.001, ****p < 0.00001.

(C) OCT4 and SOX2 proteins are reduced after rRNA transcription inhibition and translation inhibition.

(D) Gene expression changes after *DDX18* depletion, rRNA transcription inhibition, and translation inhibition. Heatmap of FPKM values of all of the downregulated (1,001 genes, fold change <−1.5, p < 0.05) and upregulated (1,046 genes, fold change >2, p < 0.05) transcripts in *DDX18*-depleted ESCs are shown and compared with the corresponding gene expression patterns resulting from ActD or CHX treatment.

(legend continued on next page)

signals in the rDNA promoter and transcribed regions were detected only under a stringent crosslinking condition using 3% formaldehyde (Figure 2C). This enrichment was detected in WT but not *DDX18*-depleted ESCs, confirming the specificity of DDX18 ^{bio}ChIP (Figure 2G). No significant ^{bio}ChIP-seq signals were detected in other genomic regions beyond rDNA sequences (Figure 2C; Table S3). Targeting of DDX18 to the rDNA neighborhood was abolished by treatment with actinomycin D (ActD), which specifically inhibits Pol I-mediated transcription at low concentrations, but not by DRB (5,6-dichloro-1-b-D-ribofuranosylbenzimidizole), which specifically inhibits Pol II (Figure 2H). Knock down of *DDX18* significantly downregulated the steady-state abundance and transcription of *45S* pre-rRNA as shown by RT-qPCR and nuclear run-on (NRO) (Figures 2I and 2J). Similarly, the level of *45S* rRNA was also significantly reduced in *DDX18*$^{-/-}$ embryos at E3.5 (Figure 2K). These results indicate that the chromatin binding of DDX18 is dependent on rRNA transcription. Nascent transcripts and/or transcription of rRNA may recruit DDX18 to the chromatin neighborhood of rDNA, where DDX18 positively feeds back on rRNA transcription to promote ribosome biogenesis.

Inhibition of rRNA Transcription Mimics the Effect of Depleting *DDX18*

ESC differentiation is accompanied by progressively decreased expression of rRNA transcripts (Figure 3A). To investigate whether DDX18 maintains ESC self-renewal through its regulation of rRNA transcription and/or mRNA translation, we treated ESCs for 24 h with drugs that inhibit Pol I, including low doses of ActD (5 or 10 ng/mL) and CX-5461, or with the translation inhibitor cycloheximide (CHX) (Drygin et al., 2011; Zhang and Lu, 2009). We then compared the transcriptional changes induced by these treatments with changes in ESCs depleted of *DDX18*. Chronic inhibition of rRNA transcription or translation led to the decreased expression of *DDX18* by 30%–40% and pluripotency master regulators and also resulted in the global downregulation of ESC-high genes and upregulation of developmental genes (Figures 3B, 3C, S4A, and S4B), indicating that both treatments impaired ESC self-renewal.

A significant overlap of differentially expressed genes was observed between cells with depletion of *DDX18* and cells with inhibition of rRNA transcription or translation (Figures 3D and S4C; Table S1). However, the inhibition of Pol I but not of global translation led to the decreased expression of genes involved in functions related to ribosomes, translation, and the nucleolus, partially recapitulating the transcriptional effect of depleting *DDX18* in ESCs (Figures 3E and 3F). These results, together with our earlier results, are consistent with a role for DDX18 in promoting rRNA transcription and demonstrate that the effect of *DDX18* depletion on pluripotency maintenance mainly results from the inhibition of rRNA transcription and ribosome biogenesis, which consequently lead to decreased translation.

DDX18 Binds PRC2 and Modulates PRC2 Complex Formation

Next, to investigate how DDX18 promotes rRNA transcription, we purified DDX18-interacting proteins using FLAG- and biotin-mediated tandem affinity purification followed by MS in ESCs expressing DDX18^{FB} (Figure S5A). With a stringent cutoff (MS score >10 and number of unique peptides $\geq$2), we identified 379 interacting proteins. Gene Ontology (GO) analysis linked these proteins to functions related to the nucleolus and ribosome biogenesis, as well as chromatin modification and transcription (Figures 4A and S5B; Table S4). Many ribosomal assembly factors, including nucleolin (NCL) and fibrillarin (FBL), were identified as interacting with DDX18 (Figure 4A), consistent with nucleolar localization (Figures S5C and S5D) and the proposed role of DDX18 in promoting ribosome biogenesis.

We found that the entire PRC2 complex, including the four core components EZH2, SUZ12, EED, and RBBP4, as well as the regulatory components JARID2 and MTF2, are present in the DDX18 interactome (Figure 4A). Co-immunoprecipitation (coIP) analysis showed that both endogenous and exogenous DDX18 captured EZH2, SUZ12, and JARID2 (Figures 4B, 4C, and S5E). These interactions were detected in both the nucleolus and nucleoplasm (Figures S5D and S5E). Reciprocal coIP of SUZ12, EED, and JARID2 captured endogenous DDX18 (Figures 4D, 4E, and S5F). In addition, coIP of SUZ12 pulled down DDX18 in both WT and knockout (KO) ESC lines lacking either JARID2 or EZH2 (Figure 4F), suggesting that the DDX18-PRC2 interaction does not require an intact protein complex. coIP with the antibody against endogenous EZH2 failed to capture DDX18, despite the successful pulldown of JARID2 (Figure S5G). In ESCs with a FLAG-tag knocked into the endogenous *EZH2* gene locus (*EZH2*$^{FLAG\ KI}$) (data not shown), anti-FLAG EZH2$^{FLAG\ KI}$ coIP also failed to capture DDX18 but pulled down SUZ12 and JARID2 (Figure 4G). These results suggest that DDX18 binding to EZH2 may be more dynamically regulated than interactions with other components of PRC2. We then asked whether RNA and transcription may affect the DDX18-PRC2 interaction. Treatments of ESCs with RNase A or inhibitors of Pol I or II transcription significantly increased the amounts of EZH2, but not SUZ12 and JARID2, that were captured by both endogenously and exogenously tagged DDX18 (Figures 4H–4J and S5H–S5K). These results indicate that physical associations of DDX18 with PRC2 core components are not mediated by RNA. Rather, RNA and/or transcription inhibit DDX18 associations with EZH2 in PRC2.

Next, we sought to test the effect of *DDX18* knockdown on the association of EZH2 with other PRC2 components. By comparing shRNAs against DDX18 to scramble controls, we found that FLAG-IP of EZH2$^{FLAG\ KI}$ appeared to capture significantly more amounts of SUZ12 and JARID2 without altering their expression (Figures 4G and 4K). This result suggests that the depletion of *DDX18* enhances the binding of EZH2 with other PRC2 components.

(E) Expression of ribosome-associated genes is specifically coordinated with rRNA transcription. GSEA of RNA-seq data is shown.

(F) Functional annotation of the genes down- or upregulated by inhibition of rRNA transcription or translation. GO analyses of the downregulated (left panel, FPKM >1, FC <−1.5, $p < 0.05$) and upregulated (right panel, FPKM >1, FC >2, $p < 0.05$) genes in ActD- (5 ng/mL), CX-5461- (1 μM), and CHX- (10 μg/mL) treated ESCs are shown.

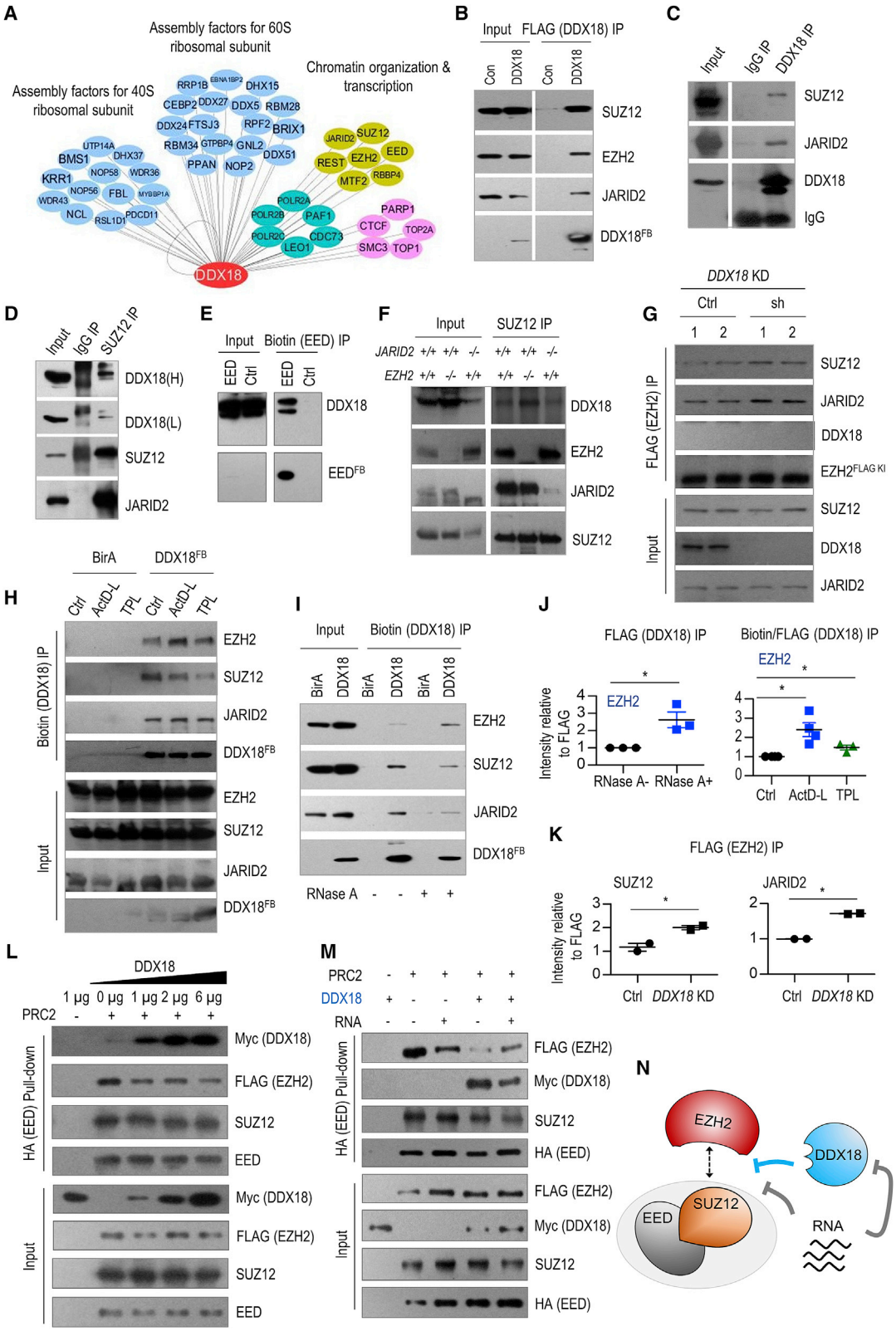

(legend on next page)

Furthermore, we purified recombinant DDX18 in 293T cells and the PRC2 complex with EZH2 (FLAG tagged), EED (hemagglutinin [HA] tagged), and SUZ12 components in a baculoviral expression system (Figures S5L and S5M) (Shen et al., 2008, 2009). We performed anti-HA-EED pull-down of the PRC2 complex and found that the addition of increasing amounts of DDX18 and/or RNA decreased the amount of EZH2 proteins that were captured by EED. These treatments had modest effects on the binding of SUZ12 to EED (Figures 4L, 4M, S5N, and S5O). Together, these *in vivo* and *in vitro* experiments demonstrate direct, physical interactions between DDX18 and PRC2 and further suggest that DDX18, along with RNA, modulate PRC2 complex formation by inhibiting EZH2 binding to other PRC2 components such as EED and SUZ12 (Figure 4N).

DDX18 Prevents PRC2 from Accessing rDNA in the Nucleolus

To visualize the DDX18-PRC2 interaction, we performed immunofluorescence staining and super-resolution structured illumination microscopy (SIM). Consistent with DDX18 ChIP under strong crosslinking conditions, we found that most DDX18 signals appeared to surround FBL-stained DFCs, in which rRNA transcription and processing occur in the nucleolus (Figures 5A and S6A). This observation supports the notion that DDX18 resides in the neighborhood of rDNA transcription units, rather than in direct contact with rDNA sequences. Despite the predominant localization of SUZ12 in the nucleoplasm, sparse yet robust SUZ12 signals were detected in the nucleolus, partially overlapping with or embedded in the DDX18-stained areas (Figure 5B). This confirms the physical DDX18-SUZ12 interaction shown by coIP.

Immunostaining of EZH2 also showed infrequent signals inside the nucleolus (Figure 5C). The knock down of *DDX18* did not alter PRC2 expression (Figure S6B), but it did dramatically increase nucleolar EZH2 signals by ~3-fold, particularly in the nucleolar peripheral region co-stained by NCL (Figures 5C and 5D). Consistently, transmission electron microscopy (TEM) detected many densely stained dark spots in the nucleolar periphery of *DDX18*-depleted ESCs (Figure 5E). These dark spots, known as nucleolar caps, are characteristic of heterochromatin (Iwamoto et al., 2008) and were observed in differentiated ESCs and other lineage-committed cells (Figure S6C). In addition, the knock down of *DDX18* dramatically altered the internal organization of the nucleolus, which became more densely stained and lost the characteristic FC, DFC, and GC structural components (Figure 5E).

ChIP-qPCR showed that the knock down of *DDX18* significantly increased the chromatin binding of EZH2 and SUZ12, as well as the repressive H3K27me2 and H3K27me3 marks, by 4- to 9-fold at the promoter and transcribed regions of rDNA, but not at developmental gene loci (Figures 6A–6D). In comparison, the removal of RNA or the inhibition of rRNA transcription failed to increase EZH2 binding at rDNA loci (Figures S6D). Thus, the observed increases in EZH2 and H3K27me3 at rDNA loci in *DDX18*-depleted cells indicate a role for the DDX18 protein in preventing PRC2 from accessing rDNA, rather than an indirect consequence of reduced transcription or RNA levels at these loci. Notably, ESC differentiation upon leukemia inhibitory factor (LIF) withdrawal for 6 days led to a ~2-fold increase in the H3K27me3 mark at rDNA loci, which is consistent with decreased rRNA transcription and DDX18 expression in differentiated ESCs (Figures 1B, 1C, 3A, and S6C). In addition, constitutive expression of exogenous DDX18 partially rescued the reduction of pre-rRNA levels during ESC differentiation (Figure S6E), supporting an active role for DDX18 in promoting rRNA transcription.

EZH2 KO Partially Rescues the Effects of DDX18 Depletion

To investigate whether DDX18 acts through PRC2 to protect the chromatin openness of rDNA loci in the maintenance of ESC self-renewal, we compared the effects of *DDX18* depletion in WT ESCs and mutant ESCs depleted of PRC2 activity (Figure 6E). KO of *EZH2* completely blocked the increase in H3K27me3 at rDNA loci induced by *DDX18* depletion (Figure 6F). Accordingly, KO of *EZH2* also partially rescued the decreased rRNA transcription and the steady-state level of *45S* rRNA in ESCs depleted of *DDX18* alone (Figures 6G and 6H). Moreover, TEM analysis showed a grossly normal nucleolar morphology upon the simultaneous depletion of *DDX18* and *EZH2*, as evidenced by the

Figure 4. DDX18 Binds PRC2 and Modulates PRC2 Complex Formation

(A) The DDX18 interactome is enriched in assembly factors for the 40S and 60S ribosomal subunits as well as proteins involved in chromatin organization and transcription.

(B and C) Validation of the physical association of DDX18 with PRC2 components. IP of exogenously expressed $DDX18^{FB}$ (B) or endogenous DDX18 (C) was used to confirm the physical interaction of DDX18 with the subunits of PRC2.

(D and E) Confirmation of the interaction between PRC2 and DDX18. Detection of the interaction between the PRC2 components and DDX18 was performed by coIP using SUZ12 (D) antibody in ESCs or by biotin-EED-IP (E) in ESC-EED^{FB}.

(F) DDX18 interacts with PRC2 independent of EZH2 and JARID2. SUZ12 coIP was used to detect the DDX18-PRC2 interaction in *EZH2* KO or *JARID2* KO ESCs.

(G) DDX18 inhibits EZH2 binding to the other components of PRC2.

(H) The effect of transcription inhibitors on the interaction between DDX18 and the components of PRC2. Biotin (DDX18) IP was performed in ActD-treated (50 ng/mL, 2 h) or triptolide-treated (Pol II inhibitor TPL, 1 μg/mL, 2 h) ESC-$DDX18^{FB}$.

(I) The effect of RNase A on the interaction between DDX18 and the components of PRC2. Detection of the interaction between DDX18 and the PRC2 components using biotin (DDX18) IP with or without RNase A treatment (25 μg/mL) in ESC-$DDX18^{FB}$.

(J) Quantitative analysis of the FLAG and biotin (DDX18) IP data shown in Figures 4H, S5H, and S5J using ImageJ.

(K) Quantitative analysis of the FLAG (EZH2) IP data in Figure 4G using ImageJ. *$p < 0.05$.

(L) DDX18 interacts with PRC2 *in vitro* and attenuates EZH2 interaction with EED-SUZ12. An HA (EED) pull-down assay was performed using PRC2 purified from insect cells with or without the addition of 1, 2, and 6 μg DDX18 protein purified from 293T cells.

(M) DDX18 or/and RNA attenuate the interaction of EZH2 with EED-SUZ12. HA (EED) pull-down with addition of DDX18 or/and RNA.

(N) A proposed model showing that DDX18 or RNA likely compromises EZH2 binding to EED and SUZ12.

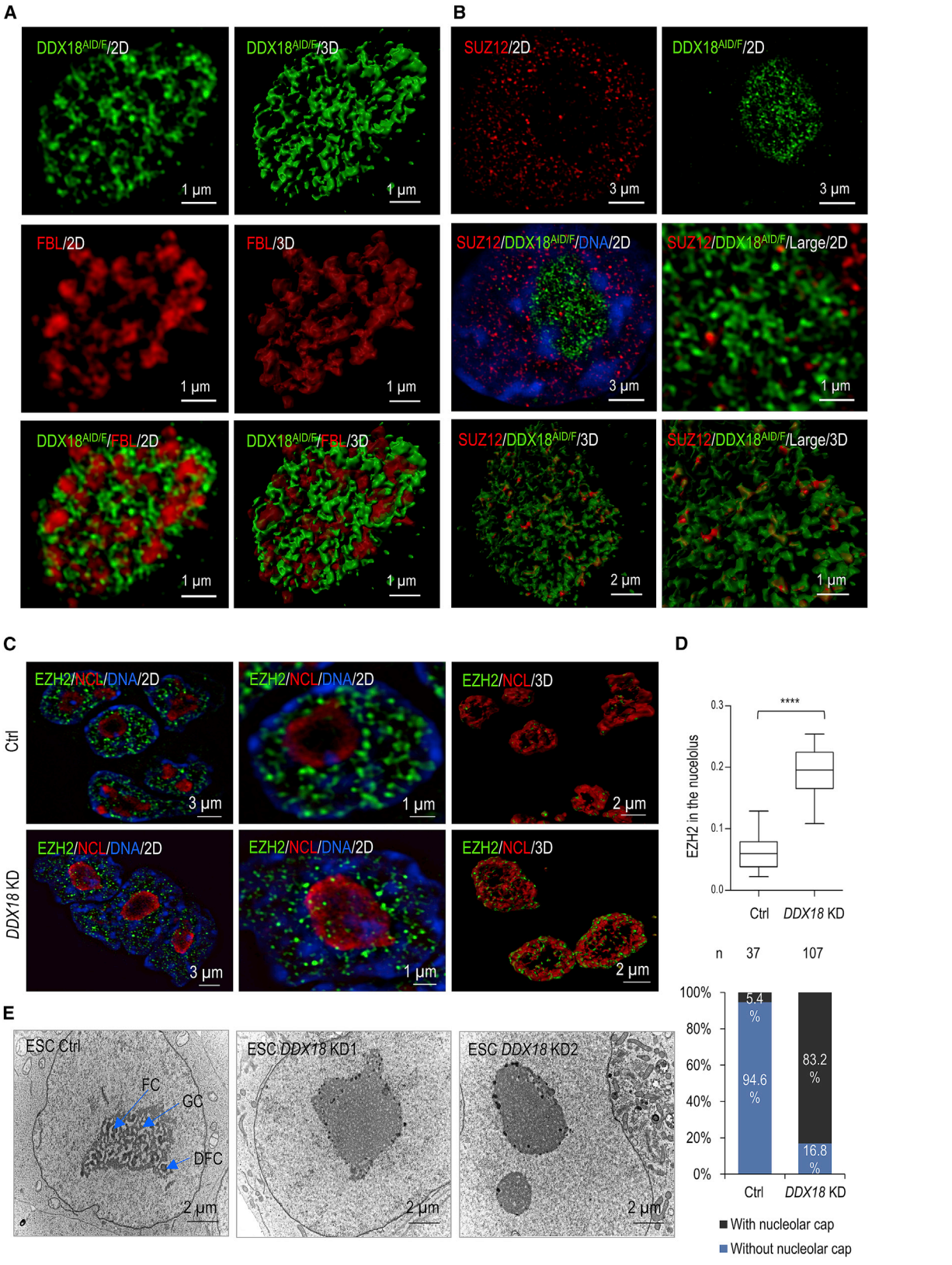

(legend on next page)

disappearance of nucleolar caps and the reappearance of organized FC, DFC, and GC structures (Figures 6I and 6J). Furthermore, the depletion of *DDX18* severely blocked ESC proliferation, which was rescued by knocking out *EZH2* (Figures 6K and 6L). ESCs depleted of both *DDX18* and *EZH2* showed better colony morphology, as indicated by distinct dome-shaped clones with smooth edges. In comparison, ESCs depleted of *DDX18* alone were flattened and spread out, which is indicative of differentiation (Figure 6K). Thus, the inhibition of PRC2 partially rescued the molecular and morphological defects caused by the depletion of *DDX18*. These results demonstrate that DDX18 safeguards ESC identity in part by antagonizing PRC2 binding to rDNA sequences to protect high-level rRNA transcription and ribosome biogenesis.

Acute Degradation of DDX18 Increases PRC2 Occupancy at rDNA

Lastly, to examine the immediate effects of DDX18 depletion on PRC2, we used the auxin-inducible degron (AID) system (Nishimura et al., 2009; Nora et al., 2017). We knocked in a 3× FLAG-fused AID tag immediately downstream of the start codon of the endogenous *DDX18* gene (designated *DDX18*$^{AID/F}$) and established homozygous knockin ESCs (Figures S7A–S7C). We subsequently infected these cells with lentivirus expressing the rice F-box protein TIR1, which recognizes the AID tag and mediates ubiquitination and proteasome-dependent degradation of DDX18$^{AID/F}$ protein in the presence of the auxin analog indole-3-acetic acid (IAA) (Figure 7A). Treatment with IAA led to an ~90% reduction at 6 h and complete degradation of the DDX18$^{AID/F}$ protein at 24 h (Figures 7B and S7D). The removal of IAA from the initial treatment for an additional 24 h allowed the recovery of DDX18$^{AID/F}$ expression (Figure 7B). We confirmed that endogenously expressed DDX18$^{AID/F}$ protein also binds nascent pre-rRNA and rDNA (Figures S7E and S7F), consistent with the analysis of ectopically tagged DDX18 (Figures 2C and 2G).

Time course analysis of nucleolar fractions upon the addition of IAA revealed that the degradation of DDX18$^{AID/F}$ led to specific increases in the amount of EZH2 protein in the nucleolus, without affecting the total levels of EZH2 in cells (Figure S7G). In subsequent analyses, we focused on the time point of 6-h treatment with IAA, presenting an early stage of DDX18$^{AID/F}$ degradation, at which no adverse effects on colony morphology and proliferation were observed (data not shown). At this time point, DDX18 binding to rDNA loci reduced by 50% (Figure S7F), whereas the binding of EZH2 and SUZ12 was significantly induced 1.5- to 7-fold at rDNA loci (Figures 7C and 7D). H3K27me3 deposition was elevated 3- to 4-fold at rDNA loci (Figure S7H). Consistently, NRO showed attenuated rRNA transcription (Figure S7I). Accompanying the recovery of DDX18 expression and binding to rDNA loci at 24 h after the removal of IAA (Figures 7B and S7F), the enrichment of EZH2, SUZ12, and H3K27me3 at rDNA loci was brought down to the normal level (Figures 7C, 7D, S7F, and S7H). Re-expression of DDX18 reversed the effect of the abnormal targeting of PRC2 at rDNA and suggests that the increased occupancy of PRC2 at rDNA is a consequence of the depletion of DDX18. Together with the knockdown results, the data from the AID-mediated rapid degradation approach led us to conclude that DDX18 inhibits the access of PRC2 to actively transcribed rDNA, independently of its effects on ESC proliferation.

DISCUSSION

Despite extensive studies of epigenetic and transcription factors, the function and regulation of ribonucleoproteins in establishing stem cell-specific programs have been underexplored. During ESC differentiation, rRNA transcription, ribosome biogenesis, and the nucleolar structure are dynamically regulated (Bi et al., 2019; Meshorer and Misteli, 2006; Niwa, 2007; Savić et al., 2014). rRNA and proteins are highly expressed in undifferentiated ESCs but are downregulated upon differentiation and in lineage-committed cells (Figure 3A) (Bi et al., 2019). However, it remains unknown whether and how these processes, once regarded as housekeeping activities, are regulated and directly contribute to stem cell pluripotency. *DDX18* was initially identified to be required for ESC viability in an RNAi screen, but its function and regulation in ESCs have not yet been studied before the present work. Here, we report an essential role for DDX18 in setting up and maintaining pluripotency during blastocyst development and in ESCs. DDX18 unexpectedly counteracts PRC2 to safeguard the chromatin openness of rDNA sequences from epigenetic silencing and consequently promotes the high levels of rRNA transcription, ribosome biogenesis, and translation that are required for ESC self-renewal. This work reveals an interplay between an essential RNA-binding protein (RBP) and a critical epigenetic regulator in governing the active euchromatic state of rDNA in transcription and stem cell regulation (Figure 7E).

The high level of DDX18 expression in pre-implantation embryos and in ESCs is consistent with hyperactive rRNA transcription and ribosome biogenesis in these embryonic cells. ESC differentiation leads to decreases in the level of DDX18 protein and in the expression of rRNA and ribosomal genes. The constitutive

Figure 5. DDX18 Prevents PRC2 from Accessing rDNA Loci and Protects the Active Chromatin Status in Nucleolus

(A) DDX18 surrounds DFC ring structures in the nucleolus. Representative SIM and 3-dimensional (3D) reconstruction images demonstrate co-staining of DDX18$^{AID/F}$ (green) and FBL (red) in ESC-DDX18$^{AID/F}$.

(B) SUZ12 partially overlaps with and is also embedded in DDX18-stained areas in the nucleolus. Representative SIM and 3D reconstruction images demonstrate co-staining of DDX18$^{AID/F}$ (green) and SUZ12 (red) in ESC-DDX18$^{AID/F}$.

(C) Super-resolution SIM imaging of EZH2 and NCL immunostaining in *DDX18*-depleted and control ESCs. Representative images show co-staining of EZH2 (green) and NCL (red) antibodies and 3D reconstructions of the co-localization of EZH2 and NCL.

(D) Statistical comparison of the ratio of the volume of EZH2 localized to the NCL-labeled nucleolus to the volume of the NCL^{+} area. Data represent 90 cells from 16 fields for controls (Ctrls) and 119 cells from 25 fields for *DDX18* KD.

(E) The nucleolar structure alters following *DDX18* depletion. Transmission electron micrographs (TEMs) show the changes in nucleolar structure following *DDX18* KD (left panel). Bar graphs show the percentage of nucleoli with or without nucleolar caps (right panel).

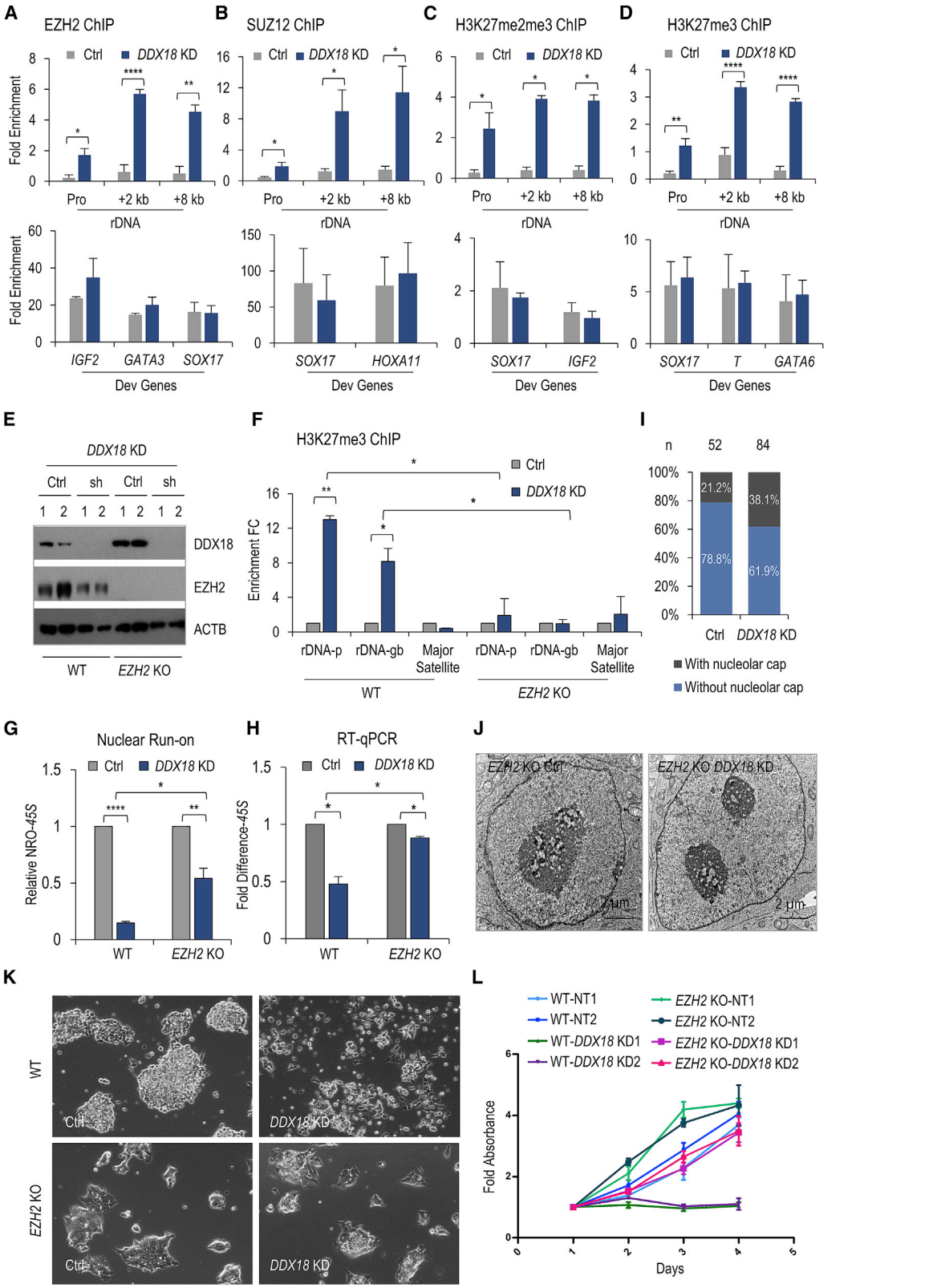

(legend on next page)

expression of DDX18 maintains rRNA transcription during differentiation. Knockdown of *DDX18* resulted in reductions in rRNA transcription, ribosome biogenesis, and pluripotency gene expression, and it also led to abnormal nucleolar morphology and loss of ESC self-renewal. In comparison, the prolonged inhibition of Pol I or translation caused downregulated *DDX18* expression and impaired ESC self-renewal. The observation of accompanied decreases in rRNA transcription and ribosomal gene expression upon DDX18 knockdown and during ESC differentiation supports the coupling of the synthesis of the RNA and protein moieties of the eukaryotic ribosome (Laferté et al., 2006). Together, these lines of evidence demonstrate that DDX18 expression is intrinsically coupled with and controls rRNA transcription and ribosome biogenesis during the maintenance of stem cell pluripotency. Downregulation of rRNA transcription not only is a consequence of reduced DDX18 expression but it also triggers ESC differentiation.

PRC2 is a well-known key executor of cell-fate transition that acts by mediating the silencing of genes that are essential for development (Faust et al., 1995; Margueron and Reinberg, 2011; O'Carroll et al., 2001; Pasini et al., 2004b). Although it is dispensable for self-renewal, PRC2 is critically required for proper ESC differentiation (Pasini et al., 2007; Shen et al., 2008, 2009). DDX18 physically interacts with PRC2 in ESCs. This association involves direct protein-protein interactions that are not mediated by RNA. Knockdown or acute degradation of DDX18 dramatically increased the nucleolar localization and binding of PRC2 to the rDNA, which was accompanied by increased H3K27me3 signals and decreased rRNA transcription. The molecular and morphological defects, particularly those related to rRNA transcription and nucleolar structure, were partially ameliorated upon the simultaneous inhibition of *EZH2* and *DDX18*. We posit that the aberrant epigenetic repression of rDNA loci together with ribogenesis deficits contribute to the phenotypes observed upon the depletion of *DDX18* in ESCs and in early embryos.

DDX18 antagonizes PRC2 to promote an open chromatin and hyperactive transcription state at rDNA loci that perpetuate the self-renewal of ESCs. However, the decreased expression of DDX18 upon ESC differentiation may allow the access of PRC2 to rDNA loci, leading to the trimethylation of H3K27 by PRC2 and reduced rRNA transcription, which consequently promotes the exit of pluripotency. We propose that the direct associations and antagonizing functions of DDX18 and PRC2 safeguard ESC self-renewal and may also allow ESCs to quickly respond to differentiation signals by reducing rRNA transcription and ribosome biogenesis, thereby facilitating the maintenance and execution of ESC pluripotency.

The nucleolus has been regarded as a phase-separated nuclear body, whose formation is driven by Pol I-mediated transcription and multivalent interactions among rRNA and ribonucleoproteins through molecular crowding (Feric et al., 2016). We speculate that distinct RNA-enriched microenvironments in the nucleolus may inhibit the entrance of PRC2, which would explain the apparent scarcity of PRC2, despite the abundance of DDX18 in the nucleolus. This hypothesis is consistent with the reported observations that the removal of RNA or the inhibition of Pol II transcription led to the increased recruitment and activity of PRC2 at Pol II target genes on the chromatin (Beltran et al., 2016; Riising et al., 2014). RNA repels PRC2 from the nucleosome and inhibits PRC2 activity (Beltran et al., 2016; Kaneko et al., 2013, 2014; Riising et al., 2014; Wang et al., 2017). Based on our results, we envision that ESCs may use two levels of regulation to prevent PRC2 from accessing the rDNA loci. First, rRNA and its transcription exclude PRC2 from the nucleolus. Second, a residual amount of PRC2 that leaks into the nucleolus is bound and sequestered by DDX18 in the outer layer of the DFC, and therefore prevented from binding to rDNA. The inhibition of Pol I or RNase treatment enhanced the binding of DDX18 to EZH2 (but not other PRC2 components) and failed to recruit PRC2 to the rDNA loci (Figures 4H–4J, S5H–S5K, and S6D). These results indicate that once PRC2 is inside the nucleolus, DDX18, rather than rRNA transcripts or transcription, plays a major role in restricting PRC2 from accessing the rDNA.

EZH2 has been reported to be an unstable component and the critical RNA-binding subunit of the PRC2 (Kaneko et al., 2013; Long et al., 2017; Pasini et al., 2004a, 2004b, 2007; Schoeftner et al., 2006). We suspect that the association of EZH2 with other components of PRC2 may be more likely to be dynamically regulated by RBPs such as DDX18 or RNA transcripts or transcription. This notion is supported by the *in vivo* and *in vitro* observations of enhanced EZH2 binding to other PRC2 components upon the depletion of *DDX18*

Figure 6. DDX18 Inhibits *De Novo* H3K27 Methylation Mediated by PRC2 at rDNA Loci, and *EZH2* KO Partially Rescues the Effects of *DDX18* Depletion

(A–D) DDX18 inhibits EZH2 occupancy and H3K27 methylation at rDNA loci. ChIP-qPCR data showing the FE of EZH2 (A), SUZ12 (B), H3K27me2me3 (C), and H3K27me3 (D) at the rDNA loci, as well as at the promoters of developmental genes, following *DDX18* depletion. Data are normalized to the *ACTB* promoter.

(E) *DDX18* is efficiently depleted in WT and *EZH2* KO ESCs.

(F) *EZH2* KO rescues the epigenetic change mediated by *DDX18* depletion. Histone H3K27 trimethylation was detected by ChIP-qPCR at rDNA loci and major satellites following *DDX18* depletion in WT and *EZH2* KO ESCs (n = 2). Data are normalized to the *ACTB* promoter, then the enrichment fold changes (FCs) are calculated by comparing KD to Ctrl.

(G and H) Inhibition of pre-rRNA (*45S*) transcription mediated by *DDX18* KD is partially rescued in *EZH2* KO ESCs, as determined by nucelar run-on (NRO) (G) and RT-qPCR (H). Unless otherwise indicated, data are presented as means ± SDs of at least 3 independent biological replicates. *$p < 0.05$, **$p < 0.001$, ****$p < 0.00001$.

(I and J) The nucleolar structural alteration mediated by *DDX18* depletion is partially rescued by the loss of EZH2. Bar graphs show the percentage of nucleoli with or without nucleolar caps (I). TEMsshow the changes in nucleolar structure following *DDX18* KD in *EZH2* KO ESCs (J).

(K and L) Morphological changes and proliferation deficits occurring upon KD of *DDX18* are partially rescued by *EZH2* deletion. Morphological observations (K) and MTT cell viability assays (L) were performed following *DDX18* KD in WT and *EZH2* KO ESCs.

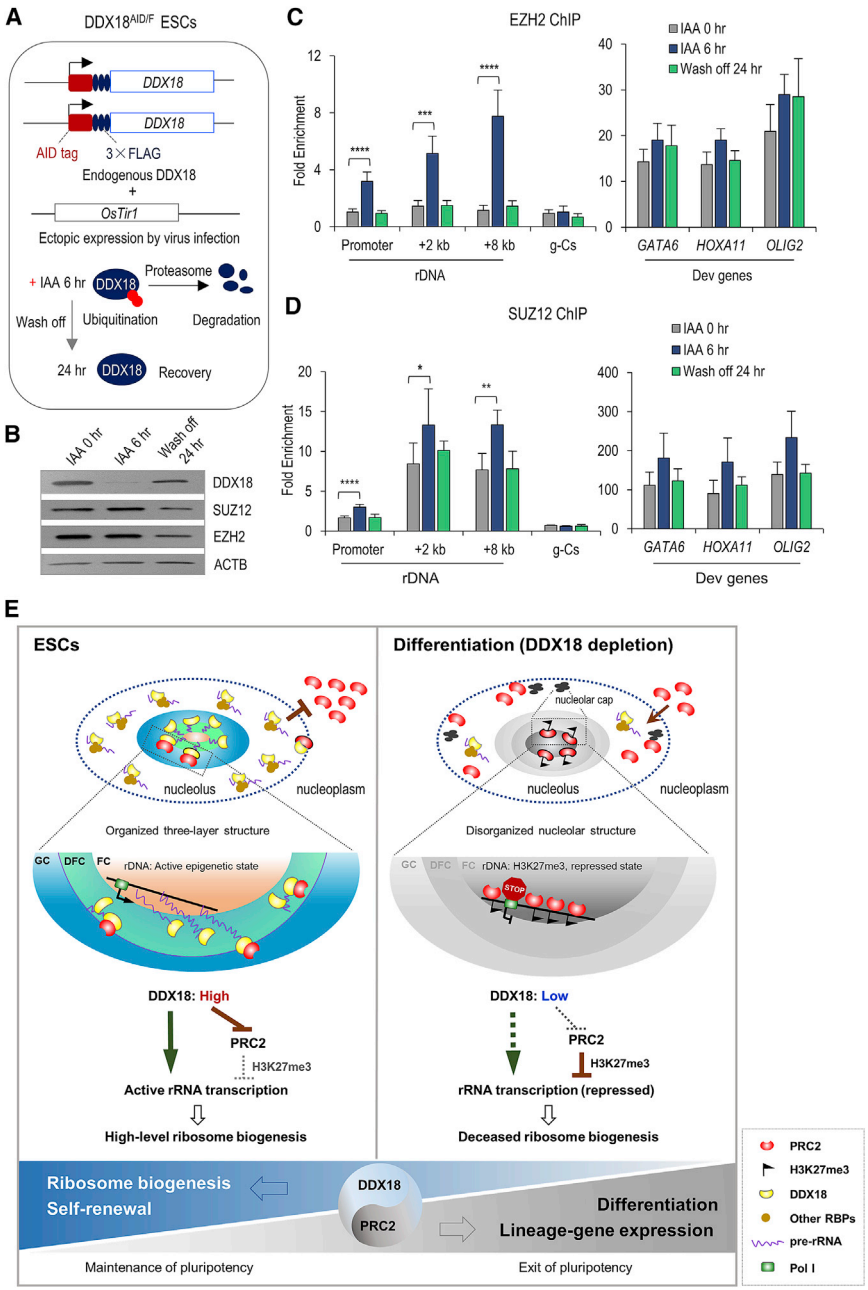

Figure 7. Acute Degradation of DDX18 Increases PRC2 Occupancy at rDNA

(A) Construction of the ESC-DDX18$^{AID/F}$ cell line.

(B) The reversible loss of DDX18 in ESC-DDX18$^{AID/F}$ cells. Western blotting demonstrates efficient depletion of DDX18 after IAA addition for 6 h, and DDX18 expression is recovered after 24 h of IAA wash off.

(C and D) DDX18 depletion immediately results in increased PRC2 occupancy at rDNA. ChIP-qPCR experiments were used to determine the FE of EZH2 (C) and SUZ12 (D) at the rDNA loci, developmental gene promoters, and negative Ctrl (*g-Cs*). Data are normalized to the *ACTB* promoter. Data are presented as means ± SDs of at least 3 independent biological replicates. *p < 0.05, **p < 0.001, ***p < 0.0001, ****p < 0.00001.

(E) A working model for DDX18 function in safeguarding rRNA transcription and ESC identity by preventing the interaction of PRC2 with rDNA loci.

and the decreased EZH2 association within PRC2 upon the addition of recombinant DDX18 or RNA (Figures 4G, 4L, and 4M). DDX18 may inhibit PRC2 complex formation in the nucleolus, consequently attenuating nucleolar PRC2 activity. It has been reported that RNA-binding proteins MOV10 and DDX5 interact with and modulate the function of PRC1 (El Messaoudi-Aubert et al., 2010; Li et al., 2017). Our results support the idea that RBPs, together with RNA and transcription, antagonize PRC2 in its chromatin-targeting and enzymatic activities (Beltran et al., 2016; Laugesen et al., 2019; Riising et al., 2014; Wiles and Selker, 2017). How exactly DDX18 affects the formation and activity of the PRC2 complex should be investigated in future studies.

In summary, our study uncovers an RBP-mediated protective mechanism to safeguard the epigenetic landscape and hyperactive transcription of rDNA in ESCs. It was reported that the nucleolus acts as an inter-chromosomal hub in global genome organization and nuclear architecture (Quinodoz et al., 2018). The abnormal activation of rRNA genes or rDNA deletions alters proper heterochromatin formation (Paredes and Maggert, 2009). Together with previous reports, our work highlights the importance of balanced rRNA transcription and ribosome

biogenesis in maintaining nucleolar integrity and ESC pluripotency.

STAR★METHODS

Detailed methods are provided in the online version of this paper and include the following:

- KEY RESOURCES TABLE
- LEAD CONTACT AND MATERIALS AVAILABLITY
- EXPERIMENTAL MODEL AND SUBJECT DETAILS
  - Animals
  - Cell lines
- METHOD DETAILS
  - CRISPR/Cas9-mediated conditional genetic deletion
  - Genotyping
  - Plasmids
  - Cell culture, transfection, and lentiviral infection
  - Quantitative real-time qPCR
  - Nuclear run-on assays
  - Immunofluorescence staining and immunoblotting
  - Isolation of nucleoli
  - Immunoprecipitation, affinity capture and mass spectrometry analysis
  - SILAC and mass spectrometry
  - Baculoviral expression and protein purification
  - Transmission electron microscopy (TEM)
  - ChIP-qPCR and ChIP-seq
  - Analysis of RNA-seq and ChIP-seq data
  - CLIP-seq and CLIP^{FB}-seq
  - MTT assay
  - Alkaline phosphatase staining
- QUANTIFICATION AND STATISTICAL ANALYSIS
- DATA AND CODE AVAILABILITY

SUPPLEMENTAL INFORMATION

Supplemental Information can be found online at https://doi.org/10.1016/j.celrep.2019.12.021.

ACKNOWLEDGMENTS

We thank Zhiguo Zhang, Qing Li, and Guojun Huang for suggestions and critical reading. We thank Elphège Nora and Benoit Bruneau for their generous gift of the IAA-inducible system containing the AID- and Ostir1-expressing plasmids. Grants are from the National Basic Research Program of China (2018YFA0107604, 2017YFA0504204), the National Natural Science Foundation of China (31630095, 31829003, and 31925015 to X.S.; 31401111 to H. Zhang), China Postdoctoral Science Foundation Grant (2014M550052 to H. Zhang) and China Postdoctoral Science Special Foundation 2015 (2015T80073 to H. Zhang).

AUTHOR CONTRIBUTIONS

X.S. conceived and supervised the study. H. Zhang found the effect of DDX18 on PRC2 and linked rRNA transcription to pluripotency. H. Zhang designed and performed the experiments with Z.W. J.Y.L. performed the bioinformatics analysis. B.H., J.W., H. Zhou, and W.X. provided critical suggestions and kind assistance. H. Zhang and X.S. wrote the manuscript with input from all of the authors.

DECLARATION OF INTERESTS

The authors declare no competing interests.

Received: June 13, 2019
Revised: October 24, 2019
Accepted: December 6, 2019
Published: January 7, 2020

REFERENCES

Beltran, M., Yates, C.M., Skalska, L., Dawson, M., Reis, F.P., Viiri, K., Fisher, C.L., Sibley, C.R., Foster, B.M., Bartke, T., et al. (2016). The interaction of PRC2 with RNA or chromatin is mutually antagonistic. Genome Res. *26*, 896–907.

Bi, X., Xu, Y., Li, T., Li, X., Li, W., Shao, W., Wang, K., Zhan, G., Wu, Z., Liu, W., et al. (2019). RNA Targets Ribogenesis Factor WDR43 to Chromatin for Transcription and Pluripotency Control. Mol. Cell *75*, 102–116.e9.

Boisvert, F.M., van Koningsbruggen, S., Navascués, J., and Lamond, A.I. (2007). The multifunctional nucleolus. Nat. Rev. Mol. Cell Biol. *8*, 574–585.

Cisterna, B., and Biggiogera, M. (2010). Ribosome biogenesis: from structure to dynamics. Int. Rev. Cell Mol. Biol. *284*, 67–111.

Cong, R., Das, S., Ugrinova, I., Kumar, S., Mongelard, F., Wong, J., and Bouvet, P. (2012). Interaction of nucleolin with ribosomal RNA genes and its role in RNA polymerase I transcription. Nucleic Acids Res. *40*, 9441–9454.

Corsini, N.S., Peer, A.M., Moeseneder, P., Roiuk, M., Burkard, T.R., Theussl, H.C., Moll, I., and Knoblich, J.A. (2018). Coordinated Control of mRNA and rRNA Processing Controls Embryonic Stem Cell Pluripotency and Differentiation. Cell Stem Cell *22*, 543–558.e12.

Dembowski, J.A., Kuo, B., and Woolford, J.L., Jr. (2013). Has1 regulates consecutive maturation and processing steps for assembly of 60S ribosomal subunits. Nucleic Acids Res. *41*, 7889–7904.

Drygin, D., Lin, A., Bliesath, J., Ho, C.B., O'Brien, S.E., Proffitt, C., Omori, M., Haddach, M., Schwaebe, M.K., Siddiqui-Jain, A., et al. (2011). Targeting RNA polymerase I with an oral small molecule CX-5461 inhibits ribosomal RNA synthesis and solid tumor growth. Cancer Res. *71*, 1418–1430.

El Messaoudi-Aubert, S., Nicholls, J., Maertens, G.N., Brookes, S., Bernstein, E., and Peters, G. (2010). Role for the MOV10 RNA helicase in polycomb-mediated repression of the INK4a tumor suppressor. Nat. Struct. Mol. Biol. *17*, 862–868.

Emery, B., de la Cruz, J., Rocak, S., Deloche, O., and Linder, P. (2004). Has1p, a member of the DEAD-box family, is required for 40S ribosomal subunit biogenesis in Saccharomyces cerevisiae. Mol. Microbiol. *52*, 141–158.

Faust, C., Schumacher, A., Holdener, B., and Magnuson, T. (1995). The eed mutation disrupts anterior mesoderm production in mice. Development *121*, 273–285.

Fazzio, T.G., Huff, J.T., and Panning, B. (2008). An RNAi screen of chromatin proteins identifies Tip60-p400 as a regulator of embryonic stem cell identity. Cell *134*, 162–174.

Feric, M., Vaidya, N., Harmon, T.S., Mitrea, D.M., Zhu, L., Richardson, T.M., Kriwacki, R.W., Pappu, R.V., and Brangwynne, C.P. (2016). Coexisting Liquid Phases Underlie Nucleolar Subcompartments. Cell *165*, 1686–1697.

Gaspar-Maia, A., Alajem, A., Meshorer, E., and Ramalho-Santos, M. (2011). Open chromatin in pluripotency and reprogramming. Nat. Rev. Mol. Cell Biol. *12*, 36–47.

Grummt, I., and Längst, G. (2013). Epigenetic control of RNA polymerase I transcription in mammalian cells. Biochim. Biophys. Acta *1829*, 393–404.

Heinz, S., Benner, C., Spann, N., Bertolino, E., Lin, Y.C., Laslo, P., Cheng, J.X., Murre, C., Singh, H., and Glass, C.K. (2010). Simple combinations of lineage-determining transcription factors prime cis-regulatory elements required for macrophage and B cell identities. Mol. Cell *38*, 576–589.

Iwamoto, F., Stadler, M., Chalupníková, K., Oakeley, E., and Nagamine, Y. (2008). Transcription-dependent nucleolar cap localization and possible nuclear function of DExH RNA helicase RHAU. Exp. Cell Res. *314*, 1378–1391.

Jankowsky, E. (2011). RNA helicases at work: binding and rearranging. Trends Biochem. Sci. *36*, 19–29.

Kaneko, S., Son, J., Shen, S.S., Reinberg, D., and Bonasio, R. (2013). PRC2 binds active promoters and contacts nascent RNAs in embryonic stem cells. Nat. Struct. Mol. Biol. *20*, 1258–1264.

Kaneko, S., Son, J., Bonasio, R., Shen, S.S., and Reinberg, D. (2014). Nascent RNA interaction keeps PRC2 activity poised and in check. Genes Dev. *28*, 1983–1988.

Laferté, A., Favry, E., Sentenac, A., Riva, M., Carles, C., and Chédin, S. (2006). The transcriptional activity of RNA polymerase I is a key determinant for the level of all ribosome components. Genes Dev. *20*, 2030–2040.

Langmead, B., and Salzberg, S.L. (2012). Fast gapped-read alignment with Bowtie 2. Nat. Methods *9*, 357–359.

Langmead, B., Hansen, K.D., and Leek, J.T. (2010). Cloud-scale RNA-sequencing differential expression analysis with Myrna. Genome Biol. *11*, R83.

Laugesen, A., Højfeldt, J.W., and Helin, K. (2019). Molecular Mechanisms Directing PRC2 Recruitment and H3K27 Methylation. Mol. Cell *74*, 8–18.

Lestrade, L., and Weber, M.J. (2006). snoRNA-LBME-db, a comprehensive database of human H/ACA and C/D box snoRNAs. Nucleic Acids Res. *34*, D158–D162.

Li, H., Lai, P., Jia, J., Song, Y., Xia, Q., Huang, K., He, N., Ping, W., Chen, J., Yang, Z., et al. (2017). RNA Helicase DDX5 Inhibits Reprogramming to Pluripotency by miRNA-Based Repression of RYBP and its PRC1-Dependent and -Independent Functions. Cell Stem Cell *20*, 462–477.e6.

Lin, C.J., Koh, F.M., Wong, P., Conti, M., and Ramalho-Santos, M. (2014). Hira-mediated H3.3 incorporation is required for DNA replication and ribosomal RNA transcription in the mouse zygote. Dev. Cell *30*, 268–279.

Linder, P., and Jankowsky, E. (2011). From unwinding to clamping - the DEAD box RNA helicase family. Nat. Rev. Mol. Cell Biol. *12*, 505–516.

Liu, L., Li, T., Song, G., He, Q., Yin, Y., Lu, J.Y., Bi, X., Wang, K., Luo, S., Chen, Y.S., et al. (2019). Insight into novel RNA-binding activities via large-scale analysis of lncRNA-bound proteome and IDH1-bound transcriptome. Nucleic Acids Res. *47*, 2244–2262.

Long, Y., Bolanos, B., Gong, L., Liu, W., Goodrich, K.J., Yang, X., Chen, S., Gooding, A.R., Maegley, K.A., Gajiwala, K.S., et al. (2017). Conserved RNA-binding specificity of polycomb repressive complex 2 is achieved by dispersed amino acid patches in EZH2. eLife *6*, e31558.

Luo, S., Lu, J.Y., Liu, L., Yin, Y., Chen, C., Han, X., Wu, B., Xu, R., Liu, W., Yan, P., et al. (2016). Divergent lncRNAs Regulate Gene Expression and Lineage Differentiation in Pluripotent Cells. Cell Stem Cell *18*, 637–652.

Margueron, R., and Reinberg, D. (2011). The Polycomb complex PRC2 and its mark in life. Nature *469*, 343–349.

McStay, B. (2016). Nucleolar organizer regions: genomic 'dark matter' requiring illumination. Genes Dev. *30*, 1598–1610.

Meshorer, E., and Misteli, T. (2006). Chromatin in pluripotent embryonic stem cells and differentiation. Nat. Rev. Mol. Cell Biol. *7*, 540–546.

Murayama, A., Ohmori, K., Fujimura, A., Minami, H., Yasuzawa-Tanaka, K., Kuroda, T., Oie, S., Daitoku, H., Okuwaki, M., Nagata, K., et al. (2008). Epigenetic control of rDNA loci in response to intracellular energy status. Cell *133*, 627–639.

Nishimura, K., Fukagawa, T., Takisawa, H., Kakimoto, T., and Kanemaki, M. (2009). An auxin-based degron system for the rapid depletion of proteins in nonplant cells. Nat. Methods *6*, 917–922.

Niwa, H. (2007). How is pluripotency determined and maintained? Development *134*, 635–646.

Nora, E.P., Goloborodko, A., Valton, A.L., Gibcus, J.H., Uebersohn, A., Abdennur, N., Dekker, J., Mirny, L.A., and Bruneau, B.G. (2017). Targeted Degradation of CTCF Decouples Local Insulation of Chromosome Domains from Genomic Compartmentalization. Cell *169*, 930–944.e22.

O'Carroll, D., Erhardt, S., Pagani, M., Barton, S.C., Surani, M.A., and Jenuwein, T. (2001). The polycomb-group gene Ezh2 is required for early mouse development. Mol. Cell. Biol. *21*, 4330–4336.

Paredes, S., and Maggert, K.A. (2009). Ribosomal DNA contributes to global chromatin regulation. Proc. Natl. Acad. Sci. USA *106*, 17829–17834.

Pasini, D., Bracken, A.P., and Helin, K. (2004a). Polycomb group proteins in cell cycle progression and cancer. Cell Cycle *3*, 396–400.

Pasini, D., Bracken, A.P., Jensen, M.R., Lazzerini Denchi, E., and Helin, K. (2004b). Suz12 is essential for mouse development and for EZH2 histone methyltransferase activity. EMBO J. *23*, 4061–4071.

Pasini, D., Bracken, A.P., Hansen, J.B., Capillo, M., and Helin, K. (2007). The polycomb group protein Suz12 is required for embryonic stem cell differentiation. Mol. Cell. Biol. *27*, 3769–3779.

Payne, E.M., Bolli, N., Rhodes, J., Abdel-Wahab, O.I., Levine, R., Hedvat, C.V., Stone, R., Khanna-Gupta, A., Sun, H., Kanki, J.P., et al. (2011). Ddx18 is essential for cell-cycle progression in zebrafish hematopoietic cells and is mutated in human AML. Blood *118*, 903–915.

Percharde, M., Bulut-Karslioglu, A., and Ramalho-Santos, M. (2017). Hypertranscription in Development, Stem Cells, and Regeneration. Dev. Cell *40*, 9–21.

Percharde, M., Lin, C.J., Yin, Y., Guan, J., Peixoto, G.A., Bulut-Karslioglu, A., Biechele, S., Huang, B., Shen, X., and Ramalho-Santos, M. (2018). A LINE1-Nucleolin Partnership Regulates Early Development and ESC Identity. Cell *174*, 391–405.e19.

Quinlan, A.R., and Hall, I.M. (2010). BEDTools: a flexible suite of utilities for comparing genomic features. Bioinformatics *26*, 841–842.

Quinodoz, S.A., Ollikainen, N., Tabak, B., Palla, A., Schmidt, J.M., Detmar, E., Lai, M.M., Shishkin, A.A., Bhat, P., Takei, Y., et al. (2018). Higher-Order Inter-chromosomal Hubs Shape 3D Genome Organization in the Nucleus. Cell *174*, 744–757.e24.

Riising, E.M., Comet, I., Leblanc, B., Wu, X., Johansen, J.V., and Helin, K. (2014). Gene silencing triggers polycomb repressive complex 2 recruitment to CpG islands genome wide. Mol. Cell *55*, 347–360.

Roberts, T.C., Hart, J.R., Kaikkonen, M.U., Weinberg, M.S., Vogt, P.K., and Morris, K.V. (2015). Quantification of nascent transcription by bromouridine immunocapture nuclear run-on RT-qPCR. Nat. Protoc. *10*, 1198–1211.

Robinson, J.T., Thorvaldsdóttir, H., Winckler, W., Guttman, M., Lander, E.S., Getz, G., and Mesirov, J.P. (2011). Integrative genomics viewer. Nat. Biotechnol. *29*, 24–26.

Savić, N., Bär, D., Leone, S., Frommel, S.C., Weber, F.A., Vollenweider, E., Ferrari, E., Ziegler, U., Kaech, A., Shakhova, O., et al. (2014). lncRNA maturation to initiate heterochromatin formation in the nucleolus is required for exit from pluripotency in ESCs. Cell Stem Cell *15*, 720–734.

Schoeftner, S., Sengupta, A.K., Kubicek, S., Mechtler, K., Spahn, L., Koseki, H., Jenuwein, T., and Wutz, A. (2006). Recruitment of PRC1 function at the initiation of X inactivation independent of PRC2 and silencing. EMBO J. *25*, 3110–3122.

Shen, X., Liu, Y., Hsu, Y.J., Fujiwara, Y., Kim, J., Mao, X., Yuan, G.C., and Orkin, S.H. (2008). EZH1 mediates methylation on histone H3 lysine 27 and complements EZH2 in maintaining stem cell identity and executing pluripotency. Mol. Cell *32*, 491–502.

Shen, X., Kim, W., Fujiwara, Y., Simon, M.D., Liu, Y., Mysliwiec, M.R., Yuan, G.C., Lee, Y., and Orkin, S.H. (2009). Jumonji modulates polycomb activity and self-renewal versus differentiation of stem cells. Cell *139*, 1303–1314.

Trapnell, C., Pachter, L., and Salzberg, S.L. (2009). TopHat: discovering splice junctions with RNA-Seq. Bioinformatics *25*, 1105–1111.

Trapnell, C., Roberts, A., Goff, L., Pertea, G., Kim, D., Kelley, D.R., Pimentel, H., Salzberg, S.L., Rinn, J.L., and Pachter, L. (2012). Differential gene and transcript expression analysis of RNA-seq experiments with TopHat and Cufflinks. Nat. Protoc. *7*, 562–578.

Uren, P.J., Bahrami-Samani, E., Burns, S.C., Qiao, M., Karginov, F.V., Hodges, E., Hannon, G.J., Sanford, J.R., Penalva, L.O., and Smith, A.D. (2012). Site

identification in high-throughput RNA-protein interaction data. Bioinformatics *28*, 3013–3020.

Wang, X., Paucek, R.D., Gooding, A.R., Brown, Z.Z., Ge, E.J., Muir, T.W., and Cech, T.R. (2017). Molecular analysis of PRC2 recruitment to DNA in chromatin and its inhibition by RNA. Nat. Struct. Mol. Biol. *24*, 1028–1038.

Wiles, E.T., and Selker, E.U. (2017). H3K27 methylation: a promiscuous repressive chromatin mark. Curr. Opin. Genet. Dev. *43*, 31–37.

Woolford, J.L., Jr., and Baserga, S.J. (2013). Ribosome biogenesis in the yeast Saccharomyces cerevisiae. Genetics *195*, 643–681.

Wu, J., Huang, B., Chen, H., Yin, Q., Liu, Y., Xiang, Y., Zhang, B., Liu, B., Wang, Q., Xia, W., et al. (2016). The landscape of accessible chromatin in mammalian preimplantation embryos. Nature *534*, 652–657.

Ying, Q.L., Stavridis, M., Griffiths, D., Li, M., and Smith, A. (2003). Conversion of embryonic stem cells into neuroectodermal precursors in adherent monoculture. Nat. Biotechnol. *21*, 183–186.

You, K.T., Park, J., and Kim, V.N. (2015). Role of the small subunit processome in the maintenance of pluripotent stem cells. Genes Dev. *29*, 2004–2009.

Zhang, Y., and Lu, H. (2009). Signaling to p53: ribosomal proteins find their way. Cancer Cell *16*, 369–377.

Zhou, Y., Schmitz, K.M., Mayer, C., Yuan, X., Akhtar, A., and Grummt, I. (2009). Reversible acetylation of the chromatin remodelling complex NoRC is required for non-coding RNA-dependent silencing. Nat. Cell Biol. *11*, 1010–1016.

Zhou, F., Li, X., Wang, W., Zhu, P., Zhou, J., He, W., Ding, M., Xiong, F., Zheng, X., Li, Z., et al. (2016). Tracing haematopoietic stem cell formation at single-cell resolution. Nature *533*, 487–492.

STAR★METHODS

KEY RESOURCES TABLE

REAGENT or RESOURCE	SOURCE	IDENTIFIER
Antibodies		
Rabbit polyclonal anti-DDX18	Bethyl Laboratories	Cat#A300-635A; RRID:AB_513611
Rabbit polyclonal anti-DDX18	Bethyl Laboratories	Cat# A300-636A, RRID:AB_2092378
Rabbit polyclonal anti-DDX18	Abcam	Cat# ab128197, RRID:AB_11143943
Rabbit polyclonal anti-DDX18	Abcam	Cat# ab70527, RRID:AB_1209631
Mouse monoclonal anti-FLAG	Sigma-Aldrich	Cat# F1804, RRID:AB_262044
Rabbit monoclonal anti-FLAG	Sigma-Aldrich	Cat# F7425, RRID:AB_439687
Mouse monoclonal anti-HA tag	Abmart	Cat# 20003,
Mouse monoclonal anti-c-Myc tag	Easybio	Cat# BE2073
Rabbit polyclonal anti-NCL	Abcam	Cat# ab22758, RRID:AB_776878
Rabbit polyclonal anti-NCL	Santa Cruz Biotech	Cat# sc-13057, RRID:AB_2229696
Rabbit polyclonal anti-FBL	Abclonal	Cat# WH079598
Rabbit polyclonal anti-JARID2	Abcam	Cat# ab102571, RRID:AB_10711410
Rabbit polyclonal anti-SUZ12	Abcam	Cat# ab77605, RRID:AB_1566775
Rabbit monoclonal anti-SUZ12	Cell Signaling Tech.	Cat# 3737, RRID:AB_2196850
Rabbit monoclonal anti-JARID2	Cell Signaling Tech.	Cat# 13594
Rabbit anti-EZH2	Cell Signaling Tech.	Cat# 5246, RRID:AB_10694683
Mouse monoclonal anti-EZH2	Cell Signaling Tech.	Cat# 3147, RRID:AB_10694383
Mouse monoclonal anti-H3K27me2me3	Active Motif	Cat# 339535
Rabbit polyclonal anti-H3K27me3	Active Motif	Cat# 39155, RRID:AB_2561020
Mouse monoclonal anti-H3K9me3	Active Motif	Cat# 61013, RRID:AB_2687870
Rabbit monoclonal anti-H3K9me2	Cell Signaling Tech.	Cat# 4658, RRID:AB_10544405
Rabbit monoclonal anti-H3K27me3	Cell Signaling Tech.	Cat# 9733, RRID:AB_2616029
Rabbit polyclonal anti-H3K4me3	Abcam	Cat# ab8580, RRID:AB_306649)
Goat polyclonal anti-Lamin B	Santa Cruz Biotech.	Cat# sc-6217, RRID:AB_648158
Mouse monoclonal anti-ACTIN	CWBiotech	Cat# CW0264M
Mouse monoclonal anti-TUBULIN	CWBiotech	Cat# CW0098M
Rabbit polyclonal anti-SOX2	Abclonal	Cat# A0561, RRID:AB_2716820
Rabbit polyclonal anti-POU5F1	Abclonal	Cat# A7920
Rabbit polyclonal anti-H3	Abclonal	Cat# A2348, RRID:AB_2631273
Goat anti-Mouse 2nd Antibody, Alexa Fluor 488	Thermo Fisher	Cat# A-11001, RRID:AB_2534069
Goat anti-Rabbit 2nd Antibody, Alexa Fluor 594	Thermo Fisher	Cat# A-11012, RRID:AB_2534079
Reagents, Chemicals and Peptides		
Actinomycin D (ActD)	Sigma Aldrich	Cat# A4262
Triptolid (TPL)	Abcam	Cat# Ab120720
Cycloheximide (CHX)	Sigma Aldrich	Cat# C7698
CX-5461	Selleck	Cat# A2684
RNase A	Takara	Cat# 740505
8% Paraformaldehyde	EMS	Cat# 157-8
Normal goat serum	Jackson	Cat# 005-000-121
Proteinase K	Merck Millipore	Cat# 539480
Protease inhibitor cocktail	Selleck	Cat# K4000
β-mercaptoethanol	Sigma Aldrich	Cat# M7522
Non-essential amino acids	Life Technologies	Cat#11140050

(*Continued on next page*)

Continued

REAGENT or RESOURCE	SOURCE	IDENTIFIER
L-Glutamine	Life Technologies	Cat# 25030081
Penicillin-streptomycin	Life Technologies	Cat#15140122
Polybrene	Sigma	Cat# 107689
Puromycin	Life Technologies	Cat#A1113802
Trizol	Thermo Fisher	Cat#15596018
3 × FLAG peptide	SciLight Peptide	Cat# C233108
Lipofectamine 3000	Thermo Fisher	Cat# L3000015
Agencourt AMPure XP	Beckman Coulter	Cat# A63881
L-Arginine-HCl	Thermo Fisher	Cat# 88427
L-Lysine-2HCl	Thermo Fisher	Cat# 88429
L-Arginine-HCl, 13C6,15N4	Cambridge Isotope Lab.	Cat# CNLM-539-H
L-Lysine-2HCl, 13C6,15N2	Cambridge Isotope Lab.	Cat# CNLM-291-H
NuPAGE Novex 4-12% Bis-Tris Gel	Thermo Fisher	Cat# NP0321BOX
Dynabeads M-280 Steptavidin	Thermo Fisher	Cat# 60210
Protein A/G UltraLink Resin	Pierce	Cat# 53133
Anti-FLAG M2 Affinity Gel	Sigma Aldrich	Cat# A2220
Pierce anti-HA agarose	Thermo Fisher	Cat# 26181
Dynabeads M-280 Steptavidin	Thermo Fisher	Cat# 60210
Dynabeads Protein A	Thermo Fisher	Cat# 10001D
iTaq Universal SYBR Green Supermix	BioRad	Cat#1725120
Critical Commercial Assays		
RevertAid First Strand cDNA Synthesis Kit	Thermo Fisher	Cat# K1622
Dynabeads mRNA purification kit	Thermo Fisher	Cat# 61006
MinElute PCR Purification Kit	QIAGEN	Cat# 28004
NBT/BCIP stock solution	Roche	Cat# 11681451001
NEBNext Ultra II First Strand Synthesis Module	NEB	Cat# E7771L
NEBNext Ultra II Second Strand Synthesis Module	NEB	Cat# E7550L
NEBNext Ultra II DNA Library Prep Kit	NEB	Cat# E7645
Strep-Tactin XT purification system	IBA Lifesciences	Cat# 2-1201/2-1000
Colloidal Blue Staining Kit	Thermo Fisher	Cat# LC6025
Experimental Models: Cell Lines		
Human: HEK293T	ATCC	CRL-3216
Mouse: 46C ES	Austin Smith Lab	Ying et al., 2003
Mouse: CJ9 ES	Shen X lab	Luo et al., 2016
Mouse: ESC-BirA	This study	N/A
Mouse: ESC-DDX18$^{AID/F}$	This study	N/A
Mouse: FLAG-Biotin-DDX18	This study	N/A
Mouse: ESC-EZH2	This study	N/A
Mouse: ESC-EED^{FB}	This study	N/A
Mouse: ESC-EZH2 KO	Shen X lab	Shen et al., 2008
Recombinant DNA		
pLKO.1 puro	Luo et al., 2016	Addgene, # 8453
PiggyBac-FLAG-Biotin-DDX18	This study	N/A
Pst1374-N-NLS-flag-linker-Cas9	Luo et al., 2016	Addgene, # 44758
pGL3-U6-sgRNA	This study	N/A
pEF-1alpha-AID-3 × FLAG-DDX18-puro	This study	N/A
Lenti-Tir1-Blast	This study	N/A
PM-link-strep-Myc-DDX18	This study	N/A

(*Continued on next page*)

Continued		
REAGENT or RESOURCE	SOURCE	IDENTIFIER
pFastbac-FLAG-EZH2	Shen X lab	Shen et al., 2008
pFastbac-SUZ12	Shen X lab	Shen et al., 2008
pFastbac-HA-EED	Shen X lab	Shen et al., 2008
Deposited Data		
Deposited CLIP-seq, CLIP^{FB}-seq, ChIP-seq, RNA-seq datasets	Table S6	GSE124580
Oligonucleotides		
A full list of oligos	N/A	Table S5
Software and Algorithms		
ImageJ (1.51h)	NIH, Univ. of Wisc. Madison	https://imagej.nih.gov/ij/
IGV (2.4.14)	Robinson et al., 2011	https://software.broadinstitute.org/software/igv/
Graphpad Prism (7.0)	Graphpad	https://www.graphpad.com/scientific-software/prism/
Bowtie	Langmead and Salzberg, 2012	http://bowtie-bio.sourceforge.net/index.shtml
Tophat	Trapnell et al., 2009	http://ccb.jhu.edu/software/tophat/index.shtml
Cufflinks	Trapnell et al., 2012	http://cole-trapnell-lab.github.io/cufflinks/
Gene set enrichment analysis (GSEA)	Broad Institute	RRID:SCR_003199

LEAD CONTACT AND MATERIALS AVAILABLITY

Further information and requests for resources and reagents should be directed to and will be fulfilled by the Lead Contact, Dr. Xiaohua Shen (xshen@tsinghua.edu.cn).

All unique/stable reagents generated in this study are available from the Lead Contact upon request.

EXPERIMENTAL MODEL AND SUBJECT DETAILS

Animals

Mutant mice were generated by CRISPR/Cas9-mediated conditional genetic deletion. EIIa-Cre mice carry a Cre transgene under the control of the adenovirus EIIa promoter directing expression of Cre recombinase in preimplantation embryos. All animal experiments were conducted in accordance with institutional guidelines for animal welfare and approved by the Institutional Animal Care and Use Committee (IACUC) at Tsinghua University. Embryos were isolated from 6-week-old female mice at the indicated day after fertilization.

Cell lines

WT (CJ9, 46C) and *EZH2* KO ESCs were stored in the Shen laboratory and have been described previously (Luo et al., 2016; Shen et al., 2008, 2009). ESC-DDX18$^{AID/F}$ was established by co-transfection of plasmids expressing Cas9 and sgRNA (5′-GTGCAGACGGCTGGGCGGCCTGG-3′), and a plasmid containing a 5′ homology arm (HA) and a 3′ HA flanking the start codon of genomic *DDX18*. Cas9-expressing ESCs were selected by puromycin treatment for 2 days following transfection. After confirming deletion or knock-in in the cell population, ESCs were plated at a low density in 10-cm plates, and clones were picked after selection for one week. Individual ESC clones were picked, expanded, and validated by PCR genotyping and immunoblotting.

METHOD DETAILS

CRISPR/Cas9-mediated conditional genetic deletion

Homologous recombination-mediated *DDX18* conditional knockout mice were created by Casgene Biotech (Beijing, China). Mouse zygotes obtained by mating males with superovulated C57BL/6J females were injected with a mixture of *Cas9* mRNA (80 ng/μl), sgRNA (5′-CCCATCACTCGGGTTTAATGTGC-3′, 40 ng/μl), and donor vector (8 ng/μl). Microinjections were performed into the male pronucleus of fertilized oocytes. Injected zygotes were transferred into pseudopregnant female CD1 mice, and viable adult mice were obtained. Correct targeting in the resulting animals was assessed by PCR and sequencing. Mice with the floxed allele were then crossed with EIIa-Cre+ mice to generate the *DDX18* exon 7 deletion.

Genotyping

Tails from experimental mice were digested in cell lysis solution (QIAGEN, 158908) with proteinase K (Roche, 3115879001) at 55°C overnight. Following centrifugation, supernatants were transferred to a new tube containing protein precipitation solution (QIAGEN,

158912). Samples were mixed using a vortex and were centrifuged. The supernatants were then transferred to a new tube, and the DNA was precipitated using isopropanol. Samples were centrifuged, and the resulting pellet was washed twice with 70% ethanol. The pellet was dried and resuspended in ddH_2O. Genotyping was performed using a PCR-based assay that distinguishes wild-type (WT) from mutant *DDX18* alleles. PCR reactions contained a combination of 2 or 3 primers for amplification of KO- and WT-specific bands from *DDX18* exon 7. Sequencing was used to confirm deletion of *DDX18* exon 7.

Plasmids

The oligonucleotides for shRNAs targeting *DDX18* were cloned into pLKO.1-Puro vectors. A non-target shRNA plasmid was used as a negative control. Two shRNAs (5′-TTGGGTTTGAAGAAGAATTAA-3′ and 5′-ATGACGGAGATCCAGCATAAA-3′) produced the best knockdown efficiency. For overexpression of full-length *DDX18*, full-length *DDX18* was amplified from cDNA from CJ9 cells and was inserted into PB-CAG-3fb expression vectors encoding N-terminal FLAG and biotin tags.

Cell culture, transfection, and lentiviral infection

Mouse embryonic stem cells (CJ9, 46C) were grown in DMEM supplemented with 15% heat-inactivated fetal bovine serum, 1% GlutaMAX, 1% penicillin/streptomycin, 1% nucleosides, 0.1 mM 2-mercaptoethanol, 1% MEM nonessential amino acids, and 1000 U/ml recombinant leukemia inhibitory factor (LIF) at 37°C. Transfection of ESCs was performed using Lipofectamine 2000 (Invitrogen) according to the manufacturer's protocol. Lentiviral particles were produced in HEK293T cells by transient co-transfection of transfer vector constructs (pLKO.1-Puro vectors), VsVg, and Delta 8.9.

For the differentiation time course (LIF withdrawal), cells were collected by trypsin digestion, washed twice with PBS to remove residual LIF, and plated with ESC culture medium without LIF in a 100-mm culture dish. Cells were harvested for analysis of RNA or protein expression or were lysed for ChIP-qPCR experiments on days 2, 4, or 6 of differentiation.

Quantitative real-time qPCR

Tissues or cultured cells were washed with PBS and harvested in TRIzol (Life Technologies, 15596018), and total RNA was extracted as indicated. Total RNA (0.5 to 2 μg) was reverse-transcribed using the RevertAid First Strand cDNA Synthesis Kit (Fermentas, K1622) with random primers. Quantitative real-time PCR (qRT-PCR) reactions were performed using iTaq Universal SYBR Green Supermix (Bio-Rad, 1725121) on a Bio-Rad CFX384 Real Time System. To detect mRNA, pairs of primers spanning two exons were used. Gene expression was normalized to that of *GAPDH* or *ACTB*. Error bars in qRT-PCR analysis represent standard deviations of average fold changes compared to the indicated control.

Nuclear run-on assays

Nuclear run-on qPCR was performed as previously described, with some modifications (Roberts et al., 2015). For one run-on experiment, approximately 5×10^6 ESCs were harvested using trypsin and were washed with cold PBS. Cell pellets were resuspended with 1 mL of NP-40 lysis buffer (10 mM Tris-HCl, pH 7.4; 3 mM $MgCl_2$; 10 mM NaCl; and 0.5% NP-40) and incubated on ice for 5 min. After centrifugation at 300 × g for 4 min, the resulting pellet was washed with 1 mL of lysis buffer without NP-40 and resuspended in nuclei storage buffer (50 mM Tris-HCl, pH 8.3; 5 mM $MgCl_2$; 0.1 mM EDTA; and 40% glycerol). An equal volume of 2X transcription buffer (300 mM KCl; 20 mM Tris-HCl, pH 8.3; 5 mM $MgCl_2$; and 4 mM DTT, supplemented with 2 mM each of ATP, GTP, and CTP; 1 mM UTP; and 1 mM biotin-UTP) was added to the nuclei. After incubation at 30°C for 30 min, RNA was extracted using TRIzol. Approximately 50 μl of pre-equilibrated and blocked streptavidin M-280 Dynabeads (Invitrogen) were washed with PBST buffer, resuspended in 100 μl of PBSTR buffer (PBST supplemented with RNase inhibitor), and then mixed with an equal volume of purified RNA. After incubation at room temperature (RT) for 1 hour, the beads were washed three times with PBSTR buffer. The RNA was extracted using TRIzol and reverse transcribed. The resulting cDNA was quantified by RT-qPCR.

Immunofluorescence staining and immunoblotting

Cells were seeded on 22 × 22mm glass coverslips. Cultured cells were fixed using 4% paraformaldehyde. Samples were blocked with 5% normal goat serum (Jackson Immuno) with 0.3% Triton X-100 (Sigma-Aldrich) in PBS for 60 min at RT and were then incubated with primary antibodies for 1 hr at 37°C, followed by the appropriate secondary fluorescently labeled antibodies (Invitrogen, 1:1000) for 1 hour at 37°C. Nuclei were counterstained with DAPI. Images were acquired using FV1200 confocal microscopy (Olympus IX83) and N-SIM microscopy (Nikon). 3D rendering was performed using Imaris 9.0.2 software.

Immunoblotting was performed as previously described. Briefly, cells were lysed in RIPA buffer supplemented with protease and phosphatase inhibitors (Roche). Protein samples were resolved by SDS-PAGE and transferred onto PVDF membranes. Blots were incubated with primary antibodies overnight at 4°C followed by incubation with HRP-conjugated species-specific antibodies (CWBiotech, 1:5000).

The following antibodies were used for immunofluorescence (IF) and western blotting (WB): DDX18 (Bethyl Laboratories A300-635A, 300-636A, IF: 1:200; Abcam, ab128197, ab7052, WB: 1: 1000), EZH2 (Cell Signaling 3147, 5246, WB: 1:1000, IF: 1:200), NCL (Santa Cruz Biotechnology, sc13057, IF: 1:100; Abcam, ab22758, WB: 1:10000), FBL (Abclonal, WH079598, IF: 1:200),

FLAG (Sigma-Aldrich, F1804, F7425, WB: 1: 1000, IF: 1:250), JARID2 (Abcam, ab102571, WB: 1:2000), SUZ12 (Cell Signaling, 3737, WB: 1:1000), LAMIN B (Santa Cruz Biotechnology, sc6217, WB: 1:5000), TUBULIN (CWBiotech CW0098M, WB: 1:5000), ACTB (CWBiotech, CW0264M, WB: 1: 5000).

Isolation of nucleoli

ES cell pellets were collected from 8 × 15 cm dishes and suspended by gentle pipetting in 4 mL Buffer A (10 mM HEPES, pH 7.9; 10 mM KCl; 1.5 mM $MgCl_2$; 0.5 mM DTT), followed by incubation on ice for 5 min. The cell suspension was homogenized approximately 10 times using a tight pestle in a pre-cooled 7 mL Dounce tissue homogenizer while the homogenizer was kept on ice. The homogenized cells were centrifuged at 1000 rpm for 5 min at 4°C. The resulting pellets were resuspended in 2.5 mL S1 solution (0.25 M sucrose, 10 mM $MgCl_2$). Then, the resuspended pellet was layered over 2.5 mL S2 solution (0.35 M sucrose, 0.5 mM $MgCl_2$) and centrifuged at 2500 rpm for 5 min at 4°C. The clean nuclear pellet was resuspended in 2.5 mL S2 solution and sonicated in 6 × 10 s bursts (with 20 s intervals between each burst). The sonicated nuclei were viewed under a phase contrast microscope to check that there were virtually no intact cells and that the nucleoli could be readily observed as dense, refractile bodies. The sonicated sample was layered over 2.5 mL of S3 solution and centrifuged at 3500 rpm for 10 min at 4°C. The resulting pellet contained the nucleoli, while the supernatant contained the nucleoplasm. The pellet was resuspended in 0.5 mL S2 solution and centrifuged at 2500 rpm for 5 min at 4°C. The final pellet contained highly purified nucleoli.

Immunoprecipitation, affinity capture and mass spectrometry analysis

For co-immunoprecipitation experiments, ESC lysates were collected by douncing cells in lysis buffer (50 mM Tris-HCl, pH 7.5; 200 mM NaCl; 1% NP-40; 1 mM EDTA; 10% glycerol; 1 mM PMSF; and proteinase inhibitor cocktail). Protein lysates were immunoprecipitated with 1 μg antibody overnight at 4°C and incubated with 50 μl protein G Dynabeads for 1-3 h. The precipitants were washed extensively with wash buffer (50 mM Tris-Hcl, pH 7.5; 200 mM NaCl; 0.01% NP-40; 1 mM EDTA; and 10% glycerol), boiled with SDS loading buffer, and subjected to SDS-PAGE and immunoblotting. At least two independent immunoprecipitations were performed for each cell line.

ESCs stably expressing FLAG- and biotin-tagged DDX18 were used for mass spectrometry experiments. Cells containing empty vector were used as the control. ESC nuclei were collected by lysing cells in hypotonic buffer (20 mM HEPES KOH, pH 8.0; 10 mM KCl; 1.5 mM $MgCl_2$; 1 mM PMSF; and proteinase inhibitor cocktail), and the nuclear extract was douced in high-salt lysis buffer (20 mM Tris-HCl, pH 7.5; 10 mM KCl; 2 mM $MgCl_2$; 400 mM NaCl; 1 mM EDTA; 20% glycerol; 1 mM PMSF; proteinase inhibitor cocktail; and benzonase) followed by centrifugation at 14,000 × g at 4°C for 10 min. After dilution in 2X NP-200 buffer (20 mM Tris-HCl, pH 7.5; 200 mM NaCl; 1 mM EDTA; 0.5% NP-40; 10% glycerol; 1 mM PMSF; and proteinase inhibitor cocktail), the protein lysate was subjected to immunoprecipitation using M2 beads (Sigma-Aldrich) overnight at 4°C. The precipitates were washed extensively and eluted using FLAG peptides in NP-200 buffer. The eluates were then incubated with M-280 Dynabeads (Thermo Fisher) overnight at 4°C. The precipitates were washed extensively with NP-200 buffer, boiled with SDS loading buffer, and subjected to SDS-PAGE followed by colloidal blue staining (Thermo Fisher LC6025). Gel fragments were excised, washed, and sent for LC-MS/MS.

SILAC and mass spectrometry

To differentially label ESCs with light and heavy amino acids, we replaced the following components in the ES-FBS culture medium: DMEM formulated without lysine and arginine instead of DMEM, dialyzed serum instead of regular FBS, and lysine and arginine added separately to light (regular L-lysine and L-arginine) and heavy ($^{13}C_6$, $^{15}N_2$ L-lysine and $^{13}C_6$, $^{15}N_4$ L-arginine) media. All SILAC reagents were purchased from Cambridge Isotope Laboratories. Complete labeling (> 95%) was confirmed by MS before initiating the experiment. To quantitatively identify changes in protein levels upon *DDX18* depletion, cells were infected with shRNA-expressing viruses and selected with puromycin for 60 h. After washing with ice-cold PBS, the control and *DDX18*-knockdown cells were harvested and counted. An equivalent number of SILAC-labeled cells (5×10^6) were lysed and sonicated in RIPA buffer (20 mM Tris-HCl, pH 7.5; 150 mM NaCl; 1 mM EDTA; 1 mM EGTA; 1% NP-40; 1% sodium deoxycholate; and protease inhibitor cocktail) on ice. After centrifugation at 14000 rpm for 10 min at 4°C, proteins of equal number of cells were combined and the concentrations were estimated using BCA. The proteins were boiled with SDS loading buffer and subjected to SDS-PAGE followed by colloidal blue staining. Gel fragments were excised, washed, and sent for LC-MS/MS.

Baculoviral expression and protein purification

DNA encoding FLAG tagged EZH2, HA tagged EED and SUZ12 were inserted into pFASTBac vector (Invitrogen), and were expressed in the Bac-to-Bac system (Invitrogen) and purified as previously described (Shen et al., 2008). Anti-FLAG agarose beads were used for purification. DDX18 was purified using Strep-Tactin system (IBA-lifesciences) from 293T. Benzonase was used during purification of PRC2 and DDX18 to remove DNA and RNA.

Transmission electron microscopy (TEM)

For morphological analysis of cultured cells, samples were grown on 35-mm dishes and fixed with 2.5% glutaraldehyde. Samples were then dehydrated in a graded series of ethanol solutions (50%, 70%, 90%, 95%, and 100%) for 8 min each. Samples were infiltrated with and embedded in SPON12 resin. After polymerizing for 48 h at 60°C, 70-nm ultrathin sections were cut using a diamond

knife and mounted on Formvar-coated copper grids (100 mesh). The sections were double-stained with uranyl acetate and lead citrate. After air-drying, samples were examined with a transmission electron microscope (Hitachi H-7650) at an acceleration voltage of 80 kV.

ChIP-qPCR and ChIP-seq

ChIP assays were performed as previously described (Luo et al., 2016; Shen et al., 2008, 2009). In brief, ESCs were cross-linked with 1% formaldehyde for 10 min at RT and quenched with glycine (final concentration of 0.125 M) for an additional 5 min. Chromatin was sonicated (microtip sonicator, 10 s/pulse, 3.5 pulses, on ice, power set at 25%) in cell lysis buffer (50 mM Tris HCl, pH 8.1; 10 mM EDTA; 1% SDS; 1 mM PMSF; and protease inhibitor cocktail) and cleared by centrifugation at 14000 rpm for 10 min at 4°C. The lysates were diluted in dilution buffer (16.7 mM Tris HCl, pH 8.1; 167 mM NaCl; 1.2 mM EDTA; 1.1% Triton X-100; 1 mM PMSF; and protease inhibitor cocktail) and incubated overnight at 4°C with the desired antibodies: anti-EZH2 (Cell Signaling 3147), anti-SUZ12 (Cell Signaling 3737), anti-histone H3K27me2me3 (Active Motif 39535), anti-histone H3K27me3 (Active Motif 39155, Cell Signaling 9733), and anti-histone H3K9me3 (Active Motif 61013). Immuno-complexes were immobilized with 20-30 μl of protein G magnetic Dynabeads (Thermo Fisher, 10001D) for 3 h at 4°C, followed by stringent washes using low-salt IP wash buffer (20 mM Tris HCl, pH 8.1; 150 mM NaCl; 1 mM EDTA; 1% Triton X-100; 0.1% SDS; and 0.1% Na-deoxycholate), high-salt IP wash buffer (20 mM Tris HCl, pH 8.1; 500 mM NaCl; 1 mM EDTA; 1% Triton X-100; 0.1% SDS; and 0.1% Na-deoxycholate), LiCl IP wash buffer (10 mM Tris HCl, pH 8.1; 250 mM LiCl; 1 mM EDTA; 0.5% NP-40; and 0.5% Na-deoxycholate), and TE buffer (10 mM Tris HCl, pH 8.1 and 1 mM EDTA). The precipitated DNA was eluted with elution buffer (9 volumes of IP elution buffer (1% SDS; 50 mM Tris HCl, pH 8.1; and 1 mM EDTA), 1 volume of 1 M $NaHCO_3$, 1/20 volume of 5 M NaCl, and 1/250 volume of proteinase K) and reverse cross-linked overnight at 65°C. DNA was purified using a DNA purification kit (QIAGEN). For biotin-DDX18-ChIP, the formaldehyde concentration was increased to 3%. Biotin-ChIP assays were performed using a similar procedure, except that the lysates were diluted in dilution buffer (16.7 mM Tris HCl, pH 8.1; 167 mM NaCl; 1.2 mM EDTA; 1.1% Triton X-100; 0.2% SDS; 1 mM PMSF; and proteinase inhibitor cocktail) and incubated overnight at 4°C with Dynabeads M-280 streptavidin (Thermo Fisher, 60210). The biotin precipitates were washed using BioChIP wash buffer 1 (2% SDS) and BioChIP wash buffer 2 (0.1 M Tris HCl, pH 8.1; 0.5 M LiCl; 1% NP-40; and 1% Na-deoxycholate). ChIP-seq libraries were prepared according to the NEBNext protocol and sequenced on an Illumina HiSeq 2500. ChIP-qPCR analyses were performed using a CFX96 or 384 Touch Real-time PCR Detection System (Bio-Rad). ChIP-qPCR signals were calculated as the percentage of input. Fold induction was calculated over *ACTB*. All primers used in qPCR analyses are shown in Table S5.

Analysis of RNA-seq and ChIP-seq data

RNA and DNA libraries were constructed by following Illumina library preparation protocols. Alignments of RNA-Seq data were performed using Tophat v2.0.10 (Trapnell et al., 2012). Only those reads uniquely mapped to the reference genome were kept for further analysis (Tophat parameter "–g 1"). Fragments Per Kilobase of exon model per Million mapped reads (FPKM) were calculated by Cufflinks 2.1.1 (Trapnell et al., 2012) to represent the expression levels of transcripts. Sets of genes that were highly expressed in ESCs (95 genes), mesendoderm (marked by *brachyury* (T)-driven GFP, ME high genes, 174), neural precursor cells (marked by *SOX1*-driven GFP, NPC-high genes, 198) and associated with ribosome function (ribosomal genes, 242) were selected as previously described (Shen et al., 2008, 2009; Zhou et al., 2016). Gene set enrichment analysis (GSEA) was performed as described previously by comparing knockdown cells to the NT shRNA control cells (Shen et al., 2008, 2009). ChIP-seq reads were aligned to the mouse genome assembly (mm9) with no gaps using Bowtie2 v2.1.0 (Langmead et al., 2010). Aligned files were further converted to bedgraph files with BEDTools (Quinlan and Hall, 2010).

CLIP-seq and CLIP^{FB}-seq

The CLIP method was performed as described previously with the specific modifications outlined below. The TAP method was developed by our lab and shares most of its protocol steps with CLIP, but includes tandem purification and excludes SDS-PAGE separation. Approximately 10^7 DDX18^{FB} ESCs grown on one 15-cm plate were harvested and resuspended with 5 mL cold PBS. The cells were re-plated and crosslinked with 600 mJ/cm^2 of 254-nm UV light. Nuclei were prepared by incubating the cells in hypotonic buffer (20 mM HEPES, pH 7.5; 10 mM KCl; 1.5 mM $MgCl_2$; 1 mM EDTA; 0.2% NP-40; 10% glycerol; 1 mM DTT; 1 mM PMSF; 1/500 volume protease inhibitor cocktail, and 400 U/ml RNase inhibitor) for 4 minutes. Cells were lysed using a 26-gauge 5/8-inch needle and were briefly sonicated. The cells were incubated for 30 min on a rotator at 4°C. The lysate was treated with 30 μl RQ1 DNase at 37°C for 10 min. The insoluble pellet was centrifuged, and the supernatant was harvested. Approximately 40 μl of pre-equilibrated FLAG M2 resin (Sigma) was used for each purification. The FLAG resin was incubated with lysate overnight at 4°C, washed twice with cold CLIP lysis buffer, and washed two more times with high salt wash buffer (5 × PBS, 0.5% NP-40, 0.5% sodium deoxycholate, and 0.1% SDS). For TAP experiments, the proteins were eluted three times with 200 ng/ml 3xFLAG peptide dissolved in CLIP lysis buffer (Sigma). The eluents were pooled and incubated with 60 μl pre-equilibrated streptavidin beads (M-280, Invitrogen) for three hours. The samples were washed twice with SDS-urea wash buffer (50 mM Tris, pH 7.4; 2% SDS; and 1 M urea) and twice with SDS-high salt wash buffer (5 × PBS, 0.5% NP-40, 0.5% SDS) at room temperature. The protein-RNA complex-bound beads were washed four times with PNK buffer (50 mM Tris, pH 7.4; 10 mM $MgCl_2$; and 0.5% NP-40). RNAs were then partially digested with MNase (NEB, diluted 1:10^5) at 37°C for 10 min (mixed in an Eppendorf Thermomixer at 1200 rpm for 5 s per 30 s). The reaction was stopped

by the addition of PNK-EGTA buffer (PNK buffer with 2 mM EGTA). The beads were then washed twice with SDS-urea wash buffer and twice with PNK buffer. To dephosphorylate the RNA, the beads were treated with CIP (NEB) for 10 min at 37°C (mixed in an Eppendorf Thermomixer at 1200 rpm for 5 s per 30 s). After two more washes with PNK buffer, the pre-adenylated 3′ linker (rAppAGATCGGAAGAGCACACGTCT-NH2, Takara) was ligated with truncated T4 RNA ligase 2 (NEB) at 16°C overnight. Non-ligated 3′ linker was washed away with two washes with CLIP lysis buffer and two washes with PNK buffer. The RNAs were then phosphorylated by T4 PNK (NEB) for 10 min at 37°C. For CLIP experiments, the RNA was subjected to SDS–PAGE separation and transfer, autoradiography, ribonucleoprotein isolation, proteinase K treatment, and overnight RNA precipitation. For TAP experiments, the samples were treated with proteinase K (50 mM Tris, pH 7.4; 150 mM NaCl; 0.5% SDS; and 20 μg proteinase K) for 30 min at 37°C to elute the protein-RNA complexes. RNAs were purified and ligated with 5′ RNA adaptor (GUUCAGAGUUCUACAGUCCGACG AUC, Takara) by T4 RNA ligase (Ambion). RNAs were reverse transcribed by Superscript III with RT primer (AGACGTGTGCTCTTCCG ATCT, Takara) and amplified for 20 cycles with Q5 DNA polymerase (NEB) (Primer_Forward: GTTCAGAGTTCTACAGTCCGACGATC; Primer_Reverse: AGACGTGTGCTCTTCCGATCT, Takara). The library index sequences were introduced by PCR with index primers (Forward [SR primer]:

AATGATACGGCGACCACCGAGATCTACACGTTCAGAGT-TCTACAGTCCGAC,

Reverse: CAAGCAGAAGACGGCATACGAGATCGTGATGTGACTGGAGTTCAGACGTGTGCTCTTCCGATCT [the underlined hexamer indicates the Illumina index sequence, Takara]) for 8 additional cycles. Libraries underwent high-throughput sequencing on an Illumina X10 or Hiseq2500 sequencing platform.

To identify RBP binding sites from CLIP and CLIP^{FB} data, raw reads were aligned to the mouse genome assembly (mm10) by Bowtie2 v2.1.0 (Langmead et al., 2010). Piranha (v1.2.1) (Uren et al., 2012) was used to call peaks in all samples using the following parameters: −b 100 -d Zero Truncated Negative Binomial -p 0.001. Piranha is a statistically robust and flexible computational method for identifying binding sites from CLIP-seq data, and is applicable to all variations of CLIP-seq technology. Bedgraphs were generated with BEDTools for visualization in a genome browser. CLIP and CLIP^{FB} binding sites were annotated as TSS-associated transcripts (1 kb upstream of transcription start site), 5′ UTRs, exons, introns, 3′UTRs, small noncoding RNAs (snRNA, snoRNA, and miRNA), antisense transcripts, and TTS regions (1 kb downstream of transcription terminal site). When a binding site was assigned to more than one of these regions, a priority ranking was used to determine an annotation (small noncoding RNA > 5′ UTR > 3′UTR > exon > intron > TSS-associated transcripts > TTS > antisense transcripts). Homer software was used for annotation of repeat elements (Heinz et al., 2010).

MTT assay

Cell growth rates were measured using a 3-(4, 5-dimethylthiazol-2-yl)-2, 5-diphenyltetrazolium bromide (MTT) proliferation assay. Briefly, 3000 cells were seeded in 96-well plates. Cell growth was examined at the indicated time points. Before testing, 20 μL of MTT reagent (2.5 mg/ml MTT in PBS, Amresco, Inc.) was added, and the cells were incubated for an additional 4 h at 37°C. Then, 200 μL of dissolving reagent DMSO (Amresco) was added to dissolve the formazan crystals. The absorbance was measured at a wavelength of 490 nm on a microplate reader. Pilot experiments were conducted to determine the optimal cell concentration for the experiments.

Alkaline phosphatase staining

ESCs were fixed using 2% paraformaldehyde. Buffer was prepared by adding 200 μL of the NBT/BCIP stock solution (Roche 11681451001) to 10 mL dilution buffer (0.1 M Tris-HCl, pH 9.5; 0.1 M NaCl; and 0.05 M $MgCl_2$). Diluted substrate (1 ml) was added to one well of a 6-well plate and was incubated at RT in the dark. The plate was checked every 5 minutes, and when a dark blue color appeared, the samples were washed twice with PBS to remove the substrate and then imaged.

QUANTIFICATION AND STATISTICAL ANALYSIS

Statistical analyses were carried out using Excel or R (version 3.3.0). Data are presented as mean + SD. The statistical tests are analyzed by Student's t test if not stated in the relevant figure legends. All of the statistical details can be found in the figure legends or Results.

DATA AND CODE AVAILABILITY

All high-throughput CLIP-seq, CLIP^{FB}-seq, ChIP-seq and RNA-seq data generated in this study are available at the Gene Expression Omnibus under accession code GSE124580.